LAPPEENRANTA UNIVERSITY OF TECHNOLOGY
LUT School of Energy Systems
LUT Mechanical Engineering

Nima Alaei

SUBSTRUCTURE DAMAGE DETECTION IN WIND TURBINES

Examiner: Professor Aki Mikkola

ABSTRACT

LAPPEENRANTA UNIVERSITY OF TECHNOLOGY
LUT School of Energy Systems
Mechanical Engineering – Design and Manufacturing

Nima Alaei

SUBSTRUCTURE DAMAGE DETECTION IN WIND TURBINES

Master's thesis

2016

77 pages, 55 figures, 8 tables and 2 appendices

Examiner: Professor Aki Mikkola

Keywords: Structure Identification, Structure Health Monitoring and Damage Detection

In recent years applying identification techniques to damage detection problems has received a lot of attention. Especially in structural dynamics, detecting defects is important in order to ensure the integrity of critical components. One of the challenges in damage detection procedures is that many of them are sophisticated and their implementation on large and complex systems, exhibiting numerous degrees of freedom (DOF), is computational intensive.

In this study, substructuring methodology is employed in order to reduce the required processing time for damage detection in the presence of high number of DOFs. In the proposed method, the structural model is separated into several subcomponents (also called substructures). Then the damaged substructure is identified by estimation of loads at its interface. In the next step, observations of a few DOFs are utilized to efficiently localize the defect. Since the number of observations is limited in practice, a modified Kalman estimator with global weight iteration is employed to extract information meaningful for the damage evaluation from a small set of sensors. In our approach, the Kalman filter is set up to estimate the coefficients of the substructure structural matrices such that, comparing with the nominal matrix, damage can be easily detected and localized.

A finite element model (FEM) of a beam is first is taken as an example of a mechanical assembly in order to investigate the computational efficiency of the method. Then, as a more complicated example, FEM of a 600W wind turbine rotor assembly is considered. The time response of the wind turbine is taken as simulated experiment and processed with the proposed method in order to evaluate the effect of measurement errors on the detection performance. The detection robustness and efficiency of the proposed method has been validated with the correct values.

TABLE OF CONTENTS

ACKNOWLEDGEMENTS

First, I would like to thank Bryndís Björk Elíasdóttir and Nikoloz Maghaldadze, their indispensable help and supports made me able to pass through barriers in many different stages of the thesis work.

I am grateful to Professor Aki Mikkola, for his kind support and guidance, who also initially made the possibility of doing this work. I would like to express my gratitude toward Morteza Karamooz Mahdiabadi for great discussions and brainstorming. As well, I am thankful to Professor Daniel J. Rixen for his sensational lectures, which completed my ground knowledge to do current thesis.

Last, but not least I would like to thank my family for all they have done for me.

Nima Alaei

LIST OF SYMBOLS AND ABBREVIATIONS

CPU	Central Processing Unit
DOF	Degree of Freedom
FEM	Finite Element Model
IGES	Initial Graphics Exchange Specification (IGES)
MDOF	Multi Degree of Freedom
a_{i}	Curvature parameters
$\mathbf{A}$	Matrix of system time dependent variables (same as $\mathbf{A}(t)$)
A	Cross section area
$\mathbf{B}$	Strain-displacement matrix
$\mathbf{C}$	Damping matrix
$\mathrm{C}_{\mathrm{sub}}$	Correlation for damping of the substructure
c_{i}	Damping coefficient in damping matrix, related to i$^{\mathrm{th}}$ DOF
$\mathrm{C}_{\mathrm{interface}}$	Correlation for damping of substructure interface
c_{ri}	Damping coefficient for substructured part, related to i$^{\mathrm{th}}$ DOF
$\boldsymbol{D}$	Vector of unknown time invariant system specification
$\boldsymbol{D_i}$	Estimation of the vector of unknown time invariant system specification
$\widehat{\boldsymbol{D}}_{\boldsymbol{q}}$	One specific estimation of the vector of unknowns of the system for component q (in same way $\boldsymbol{D}_p$ is for each entry of $\boldsymbol{D}$ when p is changing from 1 to L)
E	Modulus of Elasticity
f(t)	Load function
f_x	Normal forces for x direction (f_y and f_{xy} for y direction and in-plane shear forces)
f_{i}	Load acting on the i-th DOF of structure
f_{ri}	Load acting on the i-th DOF of substructure
$f_{unknown}$	Unknown excitation load
$g(\boldsymbol{X_t}, t)$	Continuous form of first derivative of state space vector with respect to time
h	Step size (Newmark integration method)
$\mathbf{H_n}$	Measurement model matrix at step n, $\mathbf{H}(\boldsymbol{X}_{\mathbf{n}}, t)$ as its function form
i	Indexing integer

I_x	Moment of inertia
$\mathbf{I_r}$	Identity matrix
k_i	Stiffness coefficient related to i-th DOF of structure
k_{ri}	Stiffness coefficient related to i-th DOF of substructure
$\mathbf{K_k}$	Kalman gain matrix
$K_{interface}$	Correlation for stiffness of substructure interface
K_{sub}	Correlation for stiffness of substructure
$\mathbf{K}$	Stiffness matrix
j	Indexing integer
l	Length of one element
L	Number of independent variables
m_i	Mass of element, related to i-th DOF of structure
m	Mass of element
m_{ri}	Mass of element, related to i-th DOF of substructure
$\mathbf{M}$	Mass matrix
n	Numbering and indexing purpose
N	Number of degrees of freedom
p	An integer number ($p \leq L$)
$\mathbf{P}$	Covariance matrix
$\mathbf{P_i}$	Covariance matrix in i-th update
$\mathbf{P_{t0}}$	Covariance matrix at time t0 ($\mathbf{P_0}$ as initial covariance matrix)
q	One specific component
$\mathbf{q_n}$	Process noise in time step n
Q_x	Bending moment in x direction (Q_y for y direction and Q_{xy} for twisting moment)
$\mathbf{r_n}$	Measurement noise in time step n
s	Number of steps
T	Total Error
t	Time
u	Horizontal position
V_x	Transversal force for x direction (V_y for y direction)
w_j	Entries of $\boldsymbol{W}$

$\boldsymbol{W}$	Subtraction of mass times acceleration from force vector, $\boldsymbol{W}$(t) as its function of time
$\boldsymbol{W_i}$	Subtraction of mass times acceleration from force vector for i-th iteration
x_i	Components of State Space vector of the system
$\dot{x}_i$	First derivative of components of State Space vector of the system with respect to time
$\boldsymbol{X}$	State Space vector of the system, $\boldsymbol{X}(t)$ in same manner is function of time
$\boldsymbol{X_n}$	State Space vector of the system in step n ($\boldsymbol{X_{n+1}}$ is the next step and $\boldsymbol{X_{n-1}}$ is the step before)
$\dot{\boldsymbol{X}}$	First derivative of State Space vector of the system with respect to time
$\ddot{\boldsymbol{X}}$	Second derivative of State Space vector of the system with respect to time
$\dot{\boldsymbol{X}}_{\boldsymbol{n}}$	First derivative of State Space vector of the system in step n ($\dot{\boldsymbol{X}}_{\boldsymbol{n+1}}$ is derivative of the next step and $\dot{\boldsymbol{X}}_{\boldsymbol{n-1}}$ is the one before)
$\ddot{\boldsymbol{X}}_{\boldsymbol{n}}$	Second derivative of State Space vector of the system in step n ($\ddot{\boldsymbol{X}}_{\boldsymbol{n+1}}$ is derivative of the next step and $\ddot{\boldsymbol{X}}_{\boldsymbol{n-1}}$ is the one before)
X_{sub}	Vector of displacement for concerned substructure (displacement seen as a state)
$\dot{X}_{sub}$	First derivative of X_{sub} with respect to time
$\ddot{X}_{sub}$	Second derivative of X_{sub} with respect to time
$\boldsymbol{X}_{\mathrm{t}}$	Time dependent state-space vector of the system
$\boldsymbol{X}_{\mathbf{t0}}$	State Space vector at the time t0 ($\mathbf{X_0}$ as initial State Space form)
$\widehat{\boldsymbol{X}}_{\mathbf{t0}}$	Mean value of $\boldsymbol{X}_{\mathbf{t0}}$
$\boldsymbol{Y}_{\mathbf{n}}$	Observation vector in time step n
z_i	Each special deflection shape
$\mathbf{Z}$	Shape function
α	Alpha multiplier in Newmark approach
β	Beta multiplier in Newmark approach
$\boldsymbol{\delta}_i$	Error optimization function
Δ	Expression for difference operator (finite difference quotient)
ϵ_i	Error function
θ_i	Rotational displacements

$\mathcal{N}$	Normal distribution symbol
ν	Translational displacement (ν_i is translational displacement for *i*-th node)
ρ	Density
$\boldsymbol{\varphi_n}$	State transition matrix for the state space model at step n
ω_i	System Eigenvalues in radian per second (first index is taken as the lowest frequency)

1 INTRODUCTION

Over last few years, there have been many efforts to improve non-destructive test methods for mechanical and civil structures. These methods have been named and categorized differently, including structure health monitoring, damage detection and structural identification. However, application of the last one is not limited to finding faults in systems, but also it is used in model updating and model analysis.

1.1 Background

Damage detection in structures is important for industry development. On the one hand, occurrence of damage is inevitable in mechanical systems, which can happen due to unexpected loadings such as gust of wind, or deterioration of structure due to fatigue phenomena [1]. On the other hand, complicated manufacturing processes for large mechanical structures are a challenge for traditional testing methods. As a result, safety requirement demand for feasible and cheap testing methods, which can detect the location of damage for further investigation and risk assessment.

Many methods have been developed both in time domain and frequency domain to achieve structure identification for civil engineering structures [2–5], although these methods have not been employed in parallel with substructuring in area of mechanical engineering such as wind turbines. One of the main challenges for classical health monitoring approaches is that they are very costly to apply on large and complex systems with high number of components.

In other criteria damage detection methods can be categorized in three principal stages; first investigation of damage existence in the system, then localization of damages in the system and finally examining severity of damage which is detected [6]. Therefore further examination of structure in concern of imperfection (like ultrasonic test) can be conducted as consequence.

High computational cost due to numerous numbers of degrees of freedom (DOFs) is a barrier to employ classical monitoring methods in large systems. As result, methods such as modal curvature analysis are not convenient to apply for these cases [7]. One of the solutions to

deal with the problem is implementation of substructuring techniques for damage detection in mechanical structures. Although almost whole damage detection techniques based on substructuring is investigated for civil structures like bridges and towers. By current market demand for manufacturing large mechanical engineering systems like multi-megawatt wind turbines these techniques seems necessary. Moreover for detection purposes in previous methods, there is need for installing a large number of sensors which make this method limited for small components. On the other hand, not all faults are delectable from general response of large system.

In recent years there has been a trend for manufacturing larger rotors for wind turbines, these multi-megawatt turbines can have the rotor diameter up to 200 meter [8]. Damage detection techniques based on substructuring is a possible solution to address industry demand for health monitoring of such structures.

In Figure 1-1 a multi megawatt turbine rotor is depicted. Although larger rotors are more complicated and more expensive to manufacture, economically it is more beneficiary to establish power grids made of larger turbines. Thanks to smaller cable network connection and efficient maintenance expenses, total cost of energy for giant turbines is relatively small, which make it reasonable for electrical power supplier to move towards larger sizes for turbine in the world market [9].

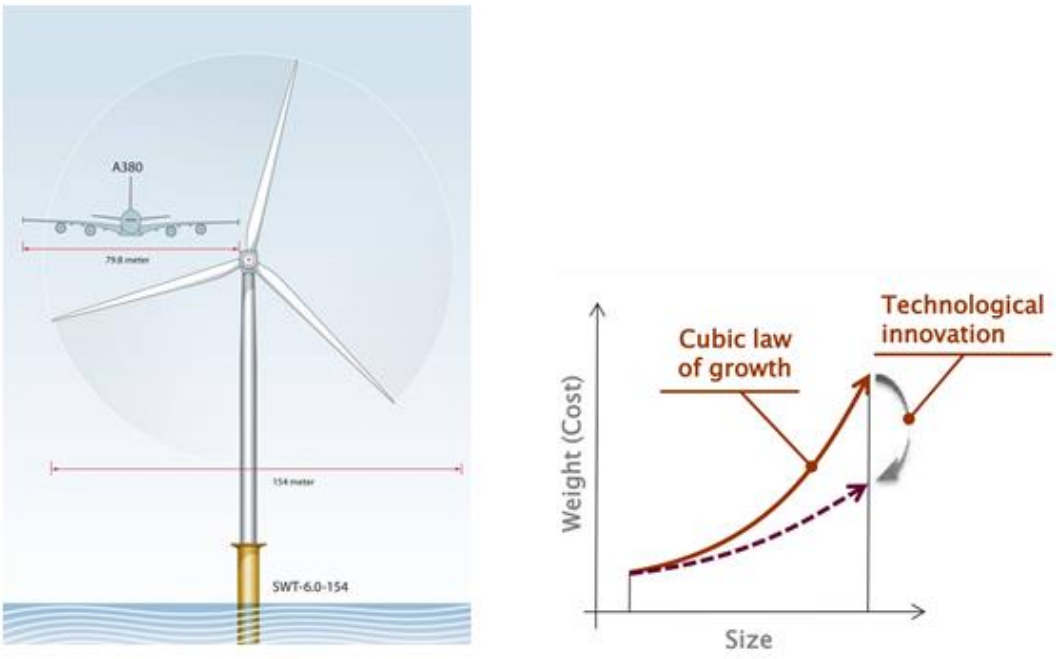

(a) (b)

Figure 1-1. Trend for large diameter rotors (a) Siemens SWT-6.0 wind turbine with 154 meter rotor diameter [10], (b) Schematic cost to size graph for wind turbine rotors [11].

In this study the substructuring approach has been used in order to efficiently estimate system parameters – mainly stiffness and damping – in presence of limited number of inputs. Kalman estimator is embedded to the method, which act based on a discrete Finite Element Model (FEM) of a mechanical system.

1.2 Motivation

As mentioned above, full measurement of DOFs for structural identification in a large dynamic mechanical system is not feasible, neither the whole structure subcomponents are required to be identified during damage detection processes. In different point of view, system excitation is also problematic for large structures, as safe excitation need a carefully studied procedure. Proposed methods for identification need to be convenient to apply for an arbitrary local part of a dynamic mechanical system. Therefore methods utilize a localized damage detection approach with incomplete observation of DOFs, are desirable for health monitoring and model updating purposes [12].

An initial system excitation is needed to collect required observation for damage detection techniques, though the excitation forces are not always known. In addition, even in

controlled laboratory conditions, it is difficult to measure exact values of excitation forces. Therefore it would be useful if the methods can estimate unknown excitation loads in the concerned subcomponent which is under identification. Challenging process of structure excitation can be neglected if the identification method is working independently from known excitation forces. This means measurements of observation can be obtained during any system natural working circumstance. Such data for identification purposes of wind turbines can be collected during natural loading cases, for example a wind gust or pilot operating conditions. Figure 1-2 has schematically illustrated purpose of current study on a spring-mass-damper system.

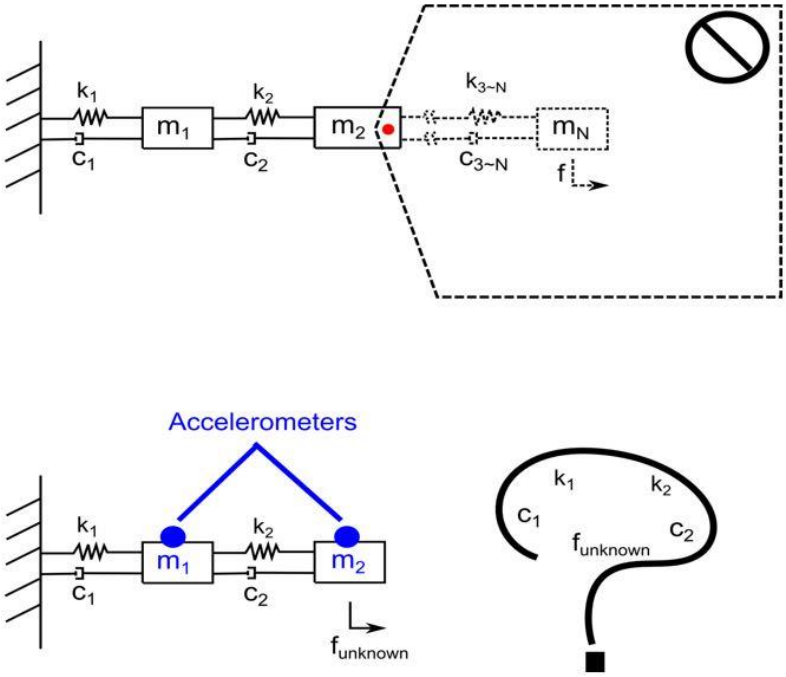

Figure 1-2. Schematic illustration for the project goal.

In the aforementioned schematic, k values are elements stiffness coefficient (for instance k_1 belongs to element 1), c values show damping coefficients, m for mass of elements and finally f represents force values on each elopement, where $f_{unknown}$ is unknown excitation load. The goal is obtaining system characteristics, including localized stiffness, damping properties up to element level. Although the system under investigation is counted to behave linearly, there is no restriction for identification of system nonlinearities parameter with application of same procedure. Red dot in the figure shows the interface node, blue colour text indicates the input data is available in the mass properties and accelerometers

observation. The mass normally is estimated based on three-dimensional spatial shape and density, meanwhile acceleration data is recorded from sensors during the excitation process.

Furthermore, experimentally measured states of the system such as accelerations are always accompanied by sensor noises. In same way, mathematical model which represents the structure can also make the simulation inaccurate in comparison with reality. It is crucial for the proposed method to remain robust in presence of process noises and measurement noises. After all, accuracy of method in identification is important, since resulted data need to be accurate enough to be used for evaluation of element degradation.

1.3 Scope

This study investigates damage detection in mechanical structures by developing Finite Element method simulation in time domain approach. System characteristics namely coefficients for stiffness and damping matrices need to be identified without assumption for initial guess values. Excitation force need to be estimated in process and not explicitly be used in the input of the process. Successful implementation is verified when estimated values are good approximation of original coefficient, which are used in simulation process. The following chapter explains methodology of the approach. Then in chapter 3 and 4, method is applied for bar and beam structures respectively. Result and modelling for an application of the method in a wind turbine is described in chapter 5. Subsequently, chapter 6 discusses results in sum and shows the possible future path based on the presented method. Last part are dedicated to bibliography and appendices.

1.4 Delimitation

This study is not developing a real laboratory test, the observation values are not recorded by accelerometers. Instead of sensors output, observation vector are calculated by numerical methods and the system model.

During identification, structure model remain linear and no permanent deformation is made. So plasticity and nonlinear behaviour is not investigated in this work, although implementation of nonlinear concepts is possible by slight modification of the currently studied method.

2 METHODOLOGY

This chapter explains concept of damage detection based on Kalman estimator. Process of damage detection can be roughly considered as following stages:

- Presenting structure with a mathematical model such as Finite Element approach
- Dividing the structure into smaller structures, so smaller part of structure can be investigated independently
- Exciting the structure and collecting observations for certain number of DOFs, in practice record of acceleration for DOFs of interest for a limited time steps which is possible in both experimental or numerical means
- Estimation of unknown excitation alongside of system parameters on the substructure which is under unknown load, based combination of Kalman estimator and least square method.

After identification of system parameters, damage can be located and monitored as a discrepancy between the expected value and identified value in stiffness of the faulty elements and the amount of damage can be compared with expected undamaged value.

2.1 State space model

This study has used concept of extended Kalman filter and substructuring as the basis for system identification. Estimation process will iterate on state vector, which contains displacement vector, velocity vector and system characteristics vector. In other words, state vector include implicit function variables, for substructure and its interface. Characteristic of system in state vector are time invariant, so only displacement and velocity of DOFs are dynamic. A schematic model of a substructure is presented in Figure 2-1. [13] Subsequently k_1, $k_2 \ldots k_n$ are stiffness coefficient values for springs in structure, then $k_{r1} \ldots k_{rm}$ are related to stiffness coefficient values substructure. In same manner, c_1, $c_2 \ldots c_n$ are damping coefficients for structure, $c_{r1} \ldots c_{rn}$ are damping coefficients for substructured part. In Figure 2-1 mass of element for the structure is presented in discrete form as m_1, $m_2 \ldots m_n$, for substructure it is shown by $m_{r1} \ldots m_{rm}$, while loads acting on the DOFs of structure are f_1, $f_2 \ldots f_n$ and $f_{r1} \ldots f_{rm}$ are loads acting on the DOFs of substructure.

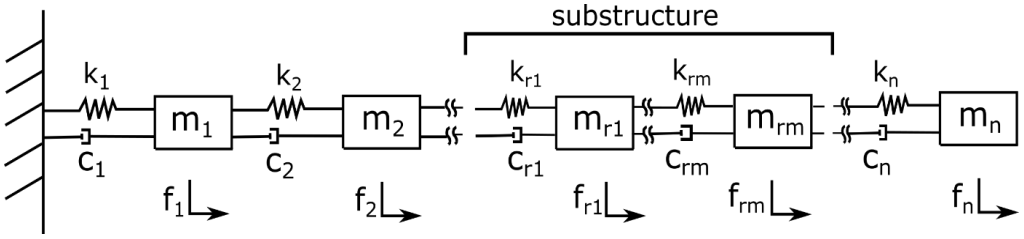

Figure 2-1. Schematic of a substructure consist of masses, springs and dampers.

Considering X_{sub} as vector of displacement for concerned substructure (here displacement can be seen as state), $\dot{X}_{sub}$ and $\ddot{X}_{sub}$ are taken as its first and second derivatives with respect to time respectively, for the concerned substructure. Then general State Space vector of the system $\boldsymbol{X}$ is formed as:

$$\boldsymbol{X} = \begin{bmatrix} X_{\text{sub}} \\ \dot{X}_{\text{sub}} \\ \text{K}_{\text{sub}} \\ \text{C}_{\text{sub}} \\ \text{K}_{\text{interface}} \\ \text{C}_{\text{interface}} \end{bmatrix} \qquad \dot{\boldsymbol{X}} = \begin{bmatrix} \dot{X}_{\text{sub}} \\ \ddot{X}_{\text{sub}} \\ 0 \\ 0 \\ 0 \\ 0 \end{bmatrix} \tag{2.1-1}$$

Where K_{sub} present correlation for stiffness of substructure, C_{sub} is correlation for damping of the substructure, $\text{K}_{\text{interface}}$ is correlation for stiffness of substructure interface and $\text{C}_{\text{interface}}$ is correlation for damping of substructure interface. In abovementioned equation $\dot{\boldsymbol{X}}$ is the first derivative of State Space vector of the system with respect to time.

2.2 Numerical integration methods

Quadrature or numerical integration is an important part in structural dynamics background. In this section theory of one dimensional integrals are discussed. The result of numerical integration is utilized in next chapter to obtain the dynamics of structure under investigation.

Newmark one step method

Differential equation of motion generally exists in continuous form, but for most of Finite Element Analysis application needs it to be solved numerically. Developed methods for numerical integration can be divided based on several criteria, according to their explicitly, step size and number of steps which is involved in calculations. A method called explicit

when solution in a time step is dependent on prior steps. In other case, if solution is dependent on current step, method is implicit.

To explain the difference between explicit and implicit method following example from a simple moving object is considered, when State Space vector of the system is presented with $\boldsymbol{X}$ vector and its first derivative is shown with $\dot{\boldsymbol{X}}$ vector one can write:

$$\boldsymbol{X}(t+\Delta t) = \boldsymbol{X}(t) + \Delta t\dot{\boldsymbol{X}}(t+\alpha\Delta t) \tag{2.2-1}$$

$$\dot{\boldsymbol{X}}(t+\Delta t) = (1-\alpha)\dot{\boldsymbol{X}}(t) + \alpha\dot{\boldsymbol{X}}(t+\alpha t) \tag{2.2-2}$$

Where t is time, Δ is presenting expression for difference operator and α is Alpha multiplier in Newmark approach. In case α is zero, State Space vector for next time step is obtained from the previous State Space and related derivative of previous time step (t) so the solution is purely explicit. When α equals to one, State Space in current step is calculated based on the current value of $\dot{\boldsymbol{X}}$ and previous State Space vector, so equation is implicit. Value of α can varies between 0 and 1, making different schemes for Newmark integration family. [14]

When the second derivative term is considered, above formulation can be written as:

$$\dot{\boldsymbol{X}}(t+\Delta t) = \dot{\boldsymbol{X}}(t) + \Delta t(1-\alpha)\ddot{\boldsymbol{X}}(t) + \alpha\ddot{\boldsymbol{X}}(t+\Delta t) \tag{2.2-3}$$

$$\boldsymbol{X}(t+\Delta t) = \boldsymbol{X}(t) + \Delta t\dot{\boldsymbol{X}}(t) + \Delta t^2\left(\frac{1}{2}-\beta\right)\ddot{\boldsymbol{X}}(t) + \Delta t^2\beta\ddot{\boldsymbol{X}}(t+\Delta t) \tag{2.2-4}$$

Where β is Beta multiplier in Newmark approach and $\ddot{\boldsymbol{X}}$ is the second derivative of State Space vector of the system with respect to time. Change of value α and β can tune integrator between purely explicit algorithms to implicit methods. In case acceleration assumed to be constant for Δt period, by considering Alpha multiplier equal to 0.5 and Beta multiplier equal to 0.25. [15]

Accuracy and stability of Newmark integration scheme

Definition for stability of an integration process is based on existence of all sub-steps, smaller than a positive non-zero step, which lead to only non-increasing set of $\boldsymbol{X}$ and $\dot{\boldsymbol{X}}$ in exact subsequent time. Also following equation are concluded:

$$\lim_{h\to 0}\frac{\dot{\boldsymbol{X}}_{n+1}-\dot{\boldsymbol{X}}_n}{h}=\lim_{h\to 0}\left[(1-\alpha)\ddot{\boldsymbol{X}}_n+\alpha\ddot{\boldsymbol{X}}_{n+1}\right]=\ddot{\boldsymbol{X}}_n \text{ or } \ddot{\boldsymbol{X}}_{n+1} \tag{2.2-5}$$

$$\lim_{h\to 0}\frac{\boldsymbol{X}_{n+1}-\boldsymbol{X}_n}{h}=\lim_{h\to 0}\left[\dot{\boldsymbol{X}}_n+\left(\frac{1}{2}-\beta\right)h\ddot{\boldsymbol{X}}_n+\beta h\ddot{\boldsymbol{X}}_{n+1}\right]=\dot{\boldsymbol{X}}_n \text{ or } \dot{\boldsymbol{X}}_{n+1} \tag{2.2-6}$$

Where $\boldsymbol{X}_n$ is State Space vector of the system in step n (n+1 subscript shows the step after n), then $\dot{\boldsymbol{X}}_n$ and $\ddot{\boldsymbol{X}}_n$ are first and second derivatives of the State Space vector of the system in step n. Meanwhile step size here is represented by h. Average constant in second derivative is considered stable for all time step sizes although accuracy of the results is crucial to achieve converged results in simulation process. Time step size for general condition is suggested to be chosen smaller than one fourth of shortest time period, as it address system dynamics which corresponds to highest system natural frequency. [16]

2.3 Bayesian Filtering

The Kalman Filtering is a method based on Bayesian filtering theory. In contradiction with classical approach in statistic, which is based on occurrence of events in random manner, Bayesian approach will not use outcome data from experiments. It will consider knowledge of system to predict set of values, when difference between observation and prediction is translated as noise. [17]

2.4 Iterated Kalman Filter

The Kalman theory has several applications in different areas of technology. It is widely used in navigation for aircraft and vehicles are most known field of its utilization. Extended Kalman works by use of model estimation of state space $\boldsymbol{X}$ in continuous form. Both the system model and measurement (complete or incomplete) required to be available [18]. It assume system model is linear for input and observation equations have Gaussian uncertainty which is translated as noise. True equation of system can be written as:

$$\boldsymbol{X}_{\mathbf{n}}=\boldsymbol{\varphi}_{\mathbf{n-1}}\boldsymbol{X}_{\mathbf{n-1}}+\mathbf{q}_{\mathbf{n-1}} \tag{2.4-1}$$

$$\boldsymbol{Y_n} = \mathbf{H_n}\boldsymbol{X_n} + \mathbf{r_n} \tag{2.4-2}$$

Where $\boldsymbol{X_n}$ is State Space vector of the system in step n, $\mathbf{q_{n-1}}$ is process noise in the step before n $\mathbf{r_n}$ is measurement noise in time step n, $\boldsymbol{\varphi_{n-1}}$ is the state transition matrix for the state space model at the step previous of the n, $\mathbf{H_n}$ is measurement model matrix and $\boldsymbol{Y_n}$ is the observation vector in time step n. [19, 20]

In the simplest form of equation when the state space vector only contains displacements and velocities and system is not subjected to external force, one can write following equation for State transition matrix form:

$$\boldsymbol{\varphi_{n-1}} = \begin{bmatrix} \mathbf{0} & \mathbf{I}_r \\ -\mathbf{M}^{-1}\mathbf{K} & -\mathbf{M}^{-1}\mathbf{C} \end{bmatrix} \tag{2.4-3}$$

Where **K** and **C** are estimated values for stiffness and damping matrixes respectively. These estimations change and is updated in each internal loop of Kalman estimator. Identity matrix is shown by $\mathbf{I}_r$**.** Lastly, **M** stands for the mass matrix.

It need to be mentioned that the Extended Kalman filter is very close to optimum for many applications, but is not exact optimum solution. That is the reason for several recent studies which worked on Kalman optimization, as example [21, 22] which proposed a generally optimum solution based on extension of Friedland's estimator [23]. He lowered the cost of augmented Kalman Filter by converting it into two filters with less order. This reduction is beneficiary for system is subjected to random bias, as it is seen in target trackers, although Friedland estimator is not remain as optimal solution in cases with dynamic noise [21].

2.5 Formulation based on Nonlinear Kalman Filter

Considering space state form, variables of system is estimated on first on a continuous form, as a function, based on time and time dependent state-space vector of the system $\boldsymbol{X_t}$**,** as it can be derived:

$$\frac{d\boldsymbol{X_t}}{dt} = g(\boldsymbol{X_t}, t) \quad \boldsymbol{X_{t0}} \sim \mathcal{N}(\widehat{\boldsymbol{X}}_{\mathbf{t0}}, \mathbf{P_{t0}}) \tag{2.5-1}$$

Where $\boldsymbol{X_{t0}}$ is State Space vector at the time t0 (is seen initial state estimation), $\widehat{\boldsymbol{X}}_{\mathbf{t0}}$ is the mean value of $\boldsymbol{X_{t0}}$ and $\mathbf{P_{t0}}$ is its covariance matrix (at time t0). Noise in $\boldsymbol{X_{t0}}$ is assumed to be Gaussian white noise and $\mathcal{N}$ is normal distribution symbol. Function g is continuous form of first derivative of state space vector with respect to time.

Subsequently, observation equation can be expressed as:

$$\boldsymbol{Y_n} = \mathbf{H}(\boldsymbol{X_n}, t) + \mathbf{r_n} \tag{2.5-2}$$

When $\boldsymbol{Y_n}$ is aforementioned observation vector in time step n which is normally collected by sensors and $\mathbf{r_n}$ is noise of the observation, $\mathbf{H}(\boldsymbol{X_n}, t)$ is the function form of $\mathbf{H_n}$ as measurement model matrix, which for this study is result of sensor noises or inaccuracy in measurement.

$$\widehat{\boldsymbol{X}}_{\boldsymbol{t}}(t_{n+1}|t_n) = \widehat{\boldsymbol{X}}_{\boldsymbol{t}}(t_n|t_n) + \int_{t_n}^{t_{n+1}} f\left(\widehat{\boldsymbol{X}}_{\boldsymbol{t}}(t_n|t_n), t\right) dt \tag{2.5-3}$$

$$\mathbf{P}(t_{n+1}|t_n) = \boldsymbol{\varphi_r}\left(t_{n+1}, t_n; \widehat{\boldsymbol{X}}_{\boldsymbol{t}}(t_n|t_n)\right)\, \mathbf{P}(t_n|t_n)\, \boldsymbol{\varphi_r}\left(\widehat{\boldsymbol{X}}_{\boldsymbol{t}}(t_n|t_n); t_{n+1}, t_n\right) \tag{2.5-4}$$

$$\widehat{\boldsymbol{X}}_{\boldsymbol{t}}(t_{n+1}|t_{n+1}) = \widehat{\boldsymbol{X}}_{\boldsymbol{t}}(t_{n+1}|t_n) + \mathbf{K_k}\left(t_{n+1}; \widehat{\boldsymbol{X}}_{\boldsymbol{t}}(t_{n+1}|t_n)\right) \ldots \tag{2.5-5}$$
$$\times \left(\boldsymbol{Y_{n+1}} - \mathbf{H}\left(\widehat{\boldsymbol{X}}_{\boldsymbol{t}}(t_{n+1}|t_n), t_{n+1}\right)\right)$$

$$\mathbf{P}(t_{n+1}|t_{n+1}) = \left(I - \mathbf{K_k}\left(t_{n+1}, t_n; \widehat{\boldsymbol{X}}_{\boldsymbol{t}}(t_{n+1}|t_n)\right)\mathbf{H}\left(t_{n+1}; \widehat{\boldsymbol{X}}_{\boldsymbol{t}}(t_{n+1}|t_n)\right)\right) \ldots \tag{2.5-6}$$
$$\times \mathbf{P}(t_{n+1}|t_n)\left(I - \mathbf{K_k}\left(t_{n+1}; \widehat{\boldsymbol{X}}_{\boldsymbol{t}}(t_{n+1}|t_n)\right)\mathbf{H}\left(t_{n+1}; \widehat{\boldsymbol{X}}_{\boldsymbol{t}}(t_{n+1}|t_n)\right)\right)^T \ldots$$
$$+\mathbf{K_k}\left(t_{n+1}; \widehat{\boldsymbol{X}}_{\boldsymbol{t}}(t_{n+1}|t_n)\right)\mathbf{r}_{n+1}\ \mathbf{K_k}\left(t_{n+1}; \widehat{\boldsymbol{X}}_{\boldsymbol{t}}(t_{n+1}|t_n)\right)^T$$

$$\mathbf{K_k}\left(t_{n+1}; \widehat{\boldsymbol{X}}_{\boldsymbol{t}}(t_{n+1}|t_n)\right) = \mathbf{P}(t_{n+1}|t_n)\,\mathbf{H}\left(t_{n+1}; \widehat{\boldsymbol{X}}_{\boldsymbol{t}}(t_{n+1}|t_n)\right)^T \ldots \tag{2.5-7}$$
$$\times \left(\mathbf{H}\left(t_{n+1}; \widehat{\boldsymbol{X}}_{\boldsymbol{t}}(t_{n+1}|t_n)\right)\mathbf{P}(t_{n+1}|t_n)\mathbf{H}\left(t_{n+1}; \widehat{\boldsymbol{X}}_{\boldsymbol{t}}(t_{n+1}|t_n)\right)^T + \mathbf{r}_{n+1}\right)^{-1}$$

Where $\mathbf{K_k}$ is Kalman gain matrix, $\mathbf{r}_{n+1}$ is noise of observation in next step, $\mathbf{P}$ is kept for covariance matrix and $\widehat{\boldsymbol{X}}_{\boldsymbol{t}}$ is the mean value. After all $t_n|t_n$ reads at time t_n with the data of time t_n, in same manner for $t_{n+1}|t_n$ which reads at time t_{n+1} by the data from time t_n.

Above mentioned formulation including sequential measurement update, time update and covariance update, can be utilized in global loop with weighting on covariance matrix for faster convergence. [24, 25]

Tuning factor is a trade-off between fast convergence and risk of losing stability. In Figure 2-2 a schematic of weighted iteration for Kalman is shown, $\mathbf{P}_i$ and $\mathbf{X}_i$ are covariance matrix and State Space vector in i-th update and index zero means at initial state ($\mathbf{P_0}$ initial covariance matrix). Alternative Kalman algorithms (e.g. Unscented-Extended Kalman) can utilize the procedure although in current literature it is developed for Kalman two-stage estimator. [26]

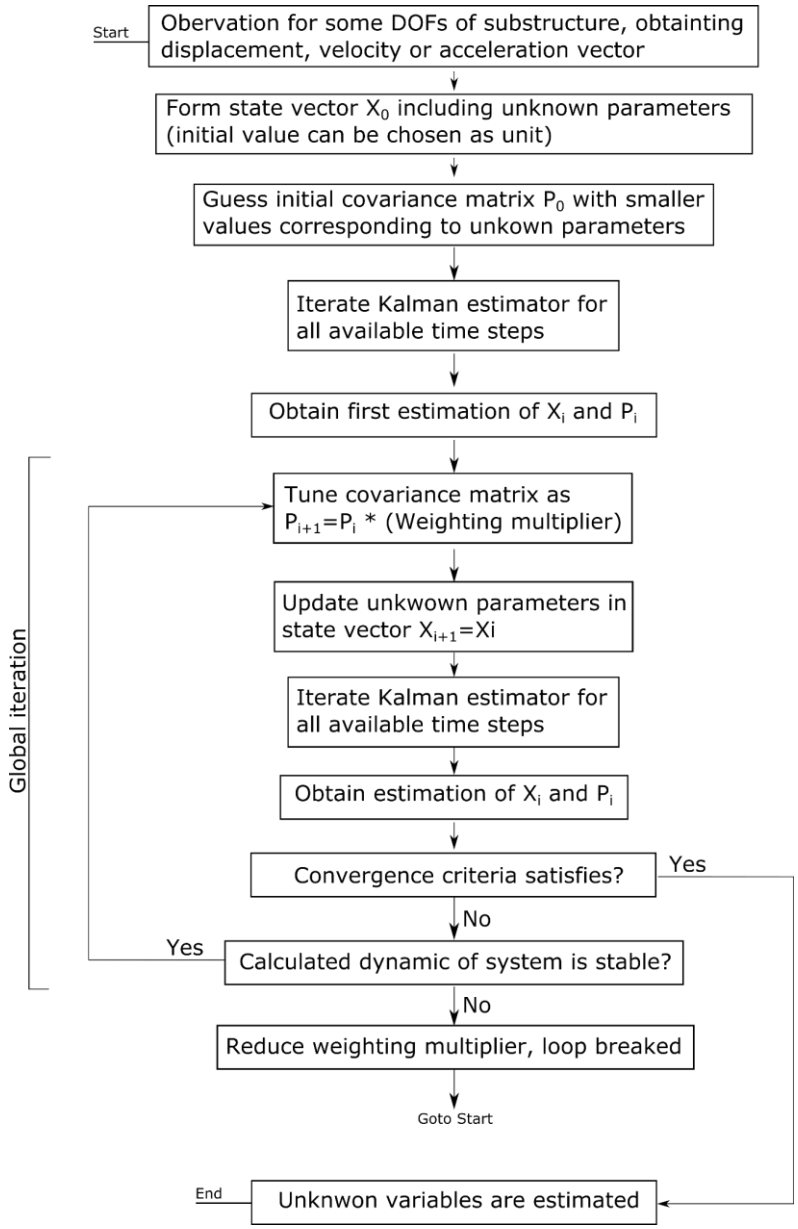

Figure 2-2. Flowchart for Kalman estimator with global weighted iteration.

Recently, modified two stage Kalman estimator is adopted from extension of Friedland estimator for optimal convergence of Kalman. Although newly introduced method is intended to optimize tracking of objects, it has been shown benefits for SI and damage detection techniques, as computational effort is decreased [21, 27, 28]. In comparison, faster convergence can be achieved by new arrangement of Kalman.

Therefore covariance update is modified to:

$$\begin{aligned}\mathbf{P}(t_{n+1}|t_{n+1}) = {} & \boldsymbol{\varphi}_{\mathbf{n}}(t_{n+1}, t_n) \times \mathbf{P}(t_n|t_n) \times \boldsymbol{\varphi}_{\mathbf{n}}(t_{n+1}, t_n)^{\mathbf{T}} \ldots \\ & - \mathbf{K}_{\boldsymbol{k}}\left(t_{n+1}, t_n; \widehat{\boldsymbol{X}}_{\boldsymbol{t}}(t_{n+1}|t_n)\right) \times \mathbf{H}\left(t_{n+1}; \widehat{\boldsymbol{X}}_{\boldsymbol{t}}(t_{n+1}|t_n)\right) \ldots \\ & \times \mathbf{P}(t_n|t_n) \times \boldsymbol{\varphi}_{\mathbf{n}}(t_{n+1}, t_n)^{\mathbf{T}}\end{aligned} \tag{2.5-8}$$

When $\boldsymbol{\varphi}_{\boldsymbol{n}}$ can be written as**:**

$$\boldsymbol{\varphi}_{\boldsymbol{n}}(t_{n+1}|t_n) = \mathbf{I}_{\boldsymbol{r}} + \mathbf{F}_{\mathbf{n}}(t_{n+1}|t_n) \tag{2.5-9}$$

And Kalman gain matrix is calculated in one stage as:

$$\begin{aligned}& \mathbf{K}_{\boldsymbol{k}}\left(t_{n+1}, t_k; \widehat{\boldsymbol{X}}_{\boldsymbol{t}}(t_{n+1}|t_n)\right) = \\ & \boldsymbol{\varphi}_{\mathbf{n}}(t_{n+1}, t_n) \times \mathbf{P}(t_n|t_n) \times \mathbf{H}\left(t_{n+1}; \widehat{\boldsymbol{X}}_{\boldsymbol{t}}(t_{n+1}|t_n)\right)^{\boldsymbol{T}} \times \ldots \\ & \left(\mathbf{H}\left(t_{n+1}; \widehat{\boldsymbol{X}}_{\boldsymbol{t}}(t_{n+1}|t_n)\right) \times \mathbf{P}(t_n|t_n) \times \mathbf{H}\left(t_{n+1}; \widehat{\boldsymbol{X}}_{\boldsymbol{t}}(t_{n+1}|t_n)\right)^{\mathbf{T}} \ldots \right. \\ & \left. + \mathbf{r}_{\boldsymbol{n+1}}\right)^{-\mathbf{1}}\end{aligned} \tag{2.5-10}$$

[21, 27, 28].

Many variation of Kalman Filter exist in the literature, such as Unscented Kalman filter which is also used for identification purposes. The main difference between approaches is number of terms in Taylor series which is used in estimation [29]. Normally the higher amount of nonlinearity in the system demands higher number of terms in Taylor series.

Tuning process is often needed for obtaining estimated parameters, also several methods for testing measurement residuals is available including normalized error square test and normalized mean error test [18].

Observability of Kalman Filtering

Before applying Kalman algorithm to a system, either as filter or estimator, observability of method needs to be considered. Simple definition of observability assumes a change in output, in response to any change in input of the system. [30]

In Kalman Filtering theory, the Kalman gain matrix is modifying state vector to forward steps, therefore if system is not observable, this defined gain will not remain study, even after infinite number of updates, as result estimator is not converged in iteration process. In conclusion, rank of $\mathbf{K}_{\boldsymbol{k}}$ as Kalman gain matrix needs to be verified for observability of observation vector [30]. In same way, for an unobservable system one or more variables from state vector matrix is indeterminate from system selected observation (in case of incomplete observation).

2.6 Iterated least square with unknown input

First step to define equation in time domain methods starts with equation of motion as series of data in time, it can be formulated as:

$$\mathbf{M}\ddot{\boldsymbol{X}}(t) + \mathbf{C}\dot{\boldsymbol{X}}(t) + \mathbf{K}\boldsymbol{X}(t) = f(t) \qquad (2.6\text{-}1)$$

Where M, C and K are representing mass, damping and stiffness matrices of system. Last term $f(t)$ is load function which excite the system. Normally mass matrix is not point of interest in estimation procedures and is considered as known data. Figure 2-3 have schematically depicted a system consisted of N number of DOFs.

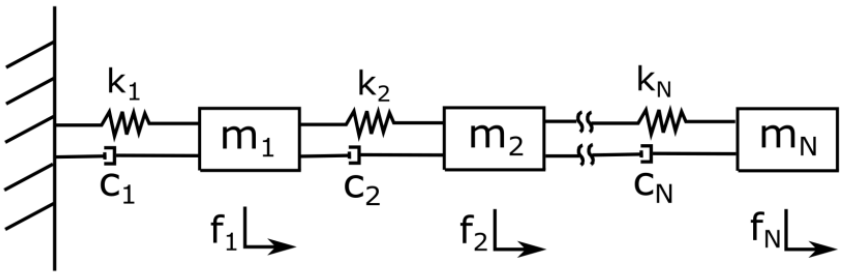

Figure 2-3. Simple mass, spring damping system with N DOFs.

Mass and stiffness matrix for a system presented in Figure 2-3 are written as:

$$\mathbf{M} = \begin{bmatrix} m_1 & 0 & \cdots & 0 \\ 0 & m_2 & \cdots & 0 \\ \vdots & \vdots & \ddots & 0 \\ 0 & 0 & \cdots & m_N \end{bmatrix} \tag{2.6-2}$$

$$\mathbf{K} = \begin{bmatrix} k_1 + k_2 & -k_2 & \cdots & 0 \\ -k_2 & k_2 + k_3 & \cdots & 0 \\ \vdots & \vdots & \ddots & \vdots \\ 0 & 0 & \cdots & k_N \end{bmatrix} \tag{2.6-3}$$

Two most used approach, viscous and Rayleigh damping, can be chosen for FEM. Viscous damping is considered in this model due to higher number of independent variables, so damping matrix is presented as:

$$\mathbf{C} = \begin{bmatrix} c_1 + c_2 & -c_2 & \cdots & 0 \\ -c_2 & c_2 + c_3 & \cdots & 0 \\ \vdots & \vdots & \ddots & \vdots \\ 0 & 0 & \cdots & c_N \end{bmatrix} \tag{2.6-4}$$

FEM need to be interpreted to other variables which make system more a suitable for iteration, in this way we define following main equation [31]:

$$\mathbf{A}(t)D(t) = \boldsymbol{W}(t) \tag{2.6-5}$$

While $\boldsymbol{F}(t)$ is written as:

$$\boldsymbol{W}(t) = f(t) - \mathbf{M}\ddot{\boldsymbol{X}}(t) \tag{2.6-6}$$

Where D is vector of unknown time invariant system specification (here stiffness and damping coefficients), **A** as matrix of system time dependent variables (dimension $N \times 2N$) is explained in following paragraph and $\boldsymbol{W}$ is a subtraction of mass times acceleration from force vector, as presented in above equation. Then assumption of viscous damping coefficients and N DOFs vector D can be written as:

$$D = [k_1, k_2, k_3 \dots k_N, c_1, c_2, c_3 \dots c_N]^T \tag{2.6-7}$$

Matrix **A** (dimension $N \times 2N$) for a simple mass spring damper model is defined by displacement and velocities as following:

$$\mathbf{A}(t) = \begin{bmatrix} x_1 & x_1 - x_2 & \dots & 0 & 0 \\ 0 & x_2 - x_1 & \dots & 0 & 0 \\ \vdots & \vdots & \vdots & \vdots & \vdots \\ 0 & 0 & \dots & x_{N-1} - x_{N-2} & x_{N-1} - x_N \\ 0 & 0 & \dots & 0 & x_N - x_{N-1} \end{bmatrix} \begin{bmatrix} \dot{x}_1 & \dot{x}_1 - \dot{x}_2 & \dots & 0 & 0 \\ 0 & \dot{x}_2 - \dot{x}_1 & \dots & 0 & 0 \\ \vdots & \vdots & \vdots & \vdots & \vdots \\ 0 & 0 & \dots & \dot{x}_{N-1} - \dot{x}_{N-2} & \dot{x}_{N-1} - \dot{x}_N \\ 0 & 0 & \dots & 0 & x_{N-1} - \dot{x}_{N-2} \end{bmatrix} \tag{2.6-8}$$

Where x_1, x_2 ... x_N are components of State Space vector of the system and $\dot{x}_1$, $\dot{x}_2$ … $\dot{x}_N$ are shown their first derivatives with respect to time. The number of time steps defines columns of $F(t)$ and number of rows meanwhile is same as number of DOFs, takes as N. [31]

Concept of least square method is straight forward, for series of data in *i*-th iteration ($\boldsymbol{W_i}$ is subtraction of mass times acceleration from force vector for i-th iteration), value of error need to be minimized. Therefore one can write for index *i* as:

$$\epsilon_i = \boldsymbol{W_i} - \mathbf{A}\boldsymbol{D_{i-1}} \tag{2.6-9}$$

$$\boldsymbol{\delta}_i = \boldsymbol{\epsilon}_i{}^T \boldsymbol{\epsilon}_i = (\boldsymbol{W}_i - \mathbf{A}\boldsymbol{D}_{i-1})^T (\boldsymbol{W}_i - \mathbf{A}\boldsymbol{D}_{i-1}) \ , \ minimum\ \boldsymbol{\delta}_i \ \rightarrow \frac{\partial \delta_i}{\partial \boldsymbol{D}_{i-1}} = 0 \quad (2.6\text{-}10)$$

Where $\boldsymbol{\delta}_i$ is error optimization function, $\boldsymbol{\epsilon}_i$ present the error function ($\boldsymbol{\epsilon}_i{}^T$ is its traspose). Then $\boldsymbol{W_i}$ represents $\boldsymbol{W}$ for each iteration and $\boldsymbol{D}_{i-1}$ (as estimation of the vector of unknown time invariant system specification) shows $\boldsymbol{D}$ is taken from previous iteration. Subsequently, $\mathbf{A}$ includes independent variables for L number of independent variables and $s \times N$ number of equations (s is number of steps, N is number of DOFs) precious main equation can be introduced as following summation:

$$\sum_{p=1}^{L} \mathbf{A}_{jp} \boldsymbol{D}_p = w_j \qquad j = 1, 2, \dots, s \times N \quad (2.6\text{-}11)$$

Where each w_j is an entry for $\boldsymbol{W}$ (which is updating in each iteration). $\boldsymbol{D}_p$ is for each entry of $\boldsymbol{D}$ when p is an integer number ($p \leq L$) which is changing from 1 to L. Total error of system in this case can be introduced as:

$$T = \sum_{j=1}^{s \times N} \left(w_j - \sum_{p=1}^{L} \mathbf{A}_{jp} \widehat{\boldsymbol{D}}_p \right) \quad (2.6\text{-}12)$$

Where $\widehat{\boldsymbol{D}}_p$ shows estimations of $\boldsymbol{D}_p$. The error term is minimized when T, as total error, is derived with respect to each specific estimation of the vector of unknowns of the system for a specific component q ($\widehat{D}_q$), as mathematically expressed as:

$$\frac{\partial T}{\partial \widehat{D}_q} = \sum_{j=1}^{s \times N} \left(w_j - \sum_{p=1}^{L} \mathbf{A}_{jp} \widehat{\boldsymbol{D}}_p \right) \mathbf{A}_{jq} = 0 \quad q = 1, 2, \dots L \quad (2.6\text{-}13)$$

Or

$$\sum_{j=1}^{s \times N} \left(\sum_{p=1}^{L} \mathbf{A}_{jp} \widehat{\boldsymbol{D}}_p \right) \mathbf{A}_{jp} = \sum_{j=1}^{s \times N} w_j \mathbf{A}_{jp} \quad q = 1, 2, \dots L \quad (2.6\text{-}14)$$

In case w_j is known, above equation will estimate L components of $\widehat{\boldsymbol{D}}_q$, but unknown variant w_j will add $s \times N$ unknown, as structure can be exposed to excitation at any N DOF and during s different time steps. Therefore it is not possible to solve the equation at one direct step, as [1]:

$$\boldsymbol{D} = (\mathbf{A}^T\,\mathbf{A})^{-1}\mathbf{A}^T\boldsymbol{W} \tag{2.6-15}$$

Solution of above equation can be obtained through iteration, but to start iteration loop it is required to know w_j for few early steps. It is not always practical to measure excitation force but as an alternative, excitation force can be taken as zero. By this assumption, iteration loop initiate with a certainly non-singular solution. Number of steps to be assumed is depends on how many of DOFs are in expose of excitation force in structure. Two time step is the minimum required steps, when force is acting on all DOFs. For special case, when only one DOF is excited, 4 initial time steps needed to assume as zero. The mentioned method can be illustrated as flowchart, in Figure 2-4 least square method iteration steps are shown.

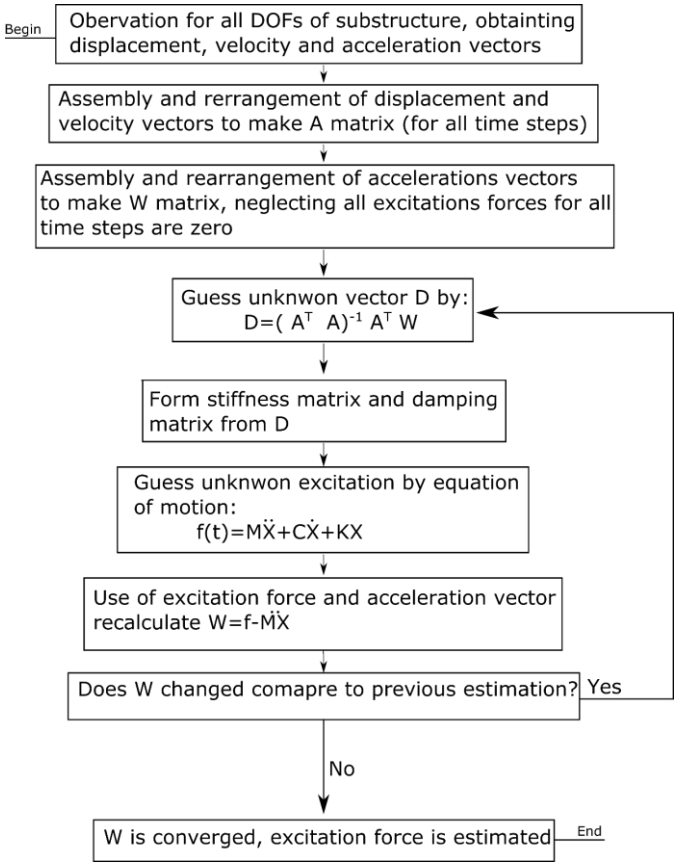

Figure 2-4. Procedure for least square estimation.

3 MODELLING AND RESULTS FOR SIMPLE STRUCTURES

In this section, previously introduced methods are applied to structure models, then results of simulation is presented. Simple structures have only one number of coupling DOF in the interfaces.

3.1 Least square for a multi DOF spring-mass-damper system

Theory for system of spring-mass-damper is presented in previous chapter. These structures are known as building model in presence of shear force. Mass of each element is considered as a concentrated point, damping is calculated based on viscous method so there are 1 independent coefficient for each DOF. Table 3-1 is presented the system characteristics for the model.

Table 3-1. System parameter for a 4 DOF spring-mass-damper system.

DOF	Mass	Stiffness	Damping
1	20	8000	32
2	10	4500	18
3	10	3500	14
4	10	3500	14

First stage in modelling is assembling mass, stiffness and damping matrices. Then equation of motion can be integrated with Newmark one step method through a time span. To define the time step size and obtain a better understanding of system, Eigenvalues of structure is calculated. These values are presented in Table 3-2, where ω presents system Eigenvalues in radian per second (first index is taken as the lowest frequency).

Table 3-2. Sorted system Eigenvalues.

	ω_1	ω_2	ω_3	ω_4
Eigenvalues (rad/s)	59.71	374.0	787.4	1253

Excitation force only act on first DOF, although it is not taken into consideration, so all other forces on three remained DOF are zero through all time steps.

Time integration verification

Dynamic of system initially calculated by numerical integration by use of Newmark method, as this algorithm is developed from theory part. It is noteworthy to mention Newmark method have advantages comparing already available function in MATLAB, since the solution can be obtained without writing equation of motion for each DOF. Validation purpose is performed by comparing solution of Newmark for displacement of first DOF in 20 second simulation time, as it is depicted in Figure 3-1 result of integration are same when ode113 and ode45 function of MATLAB are applied [32].

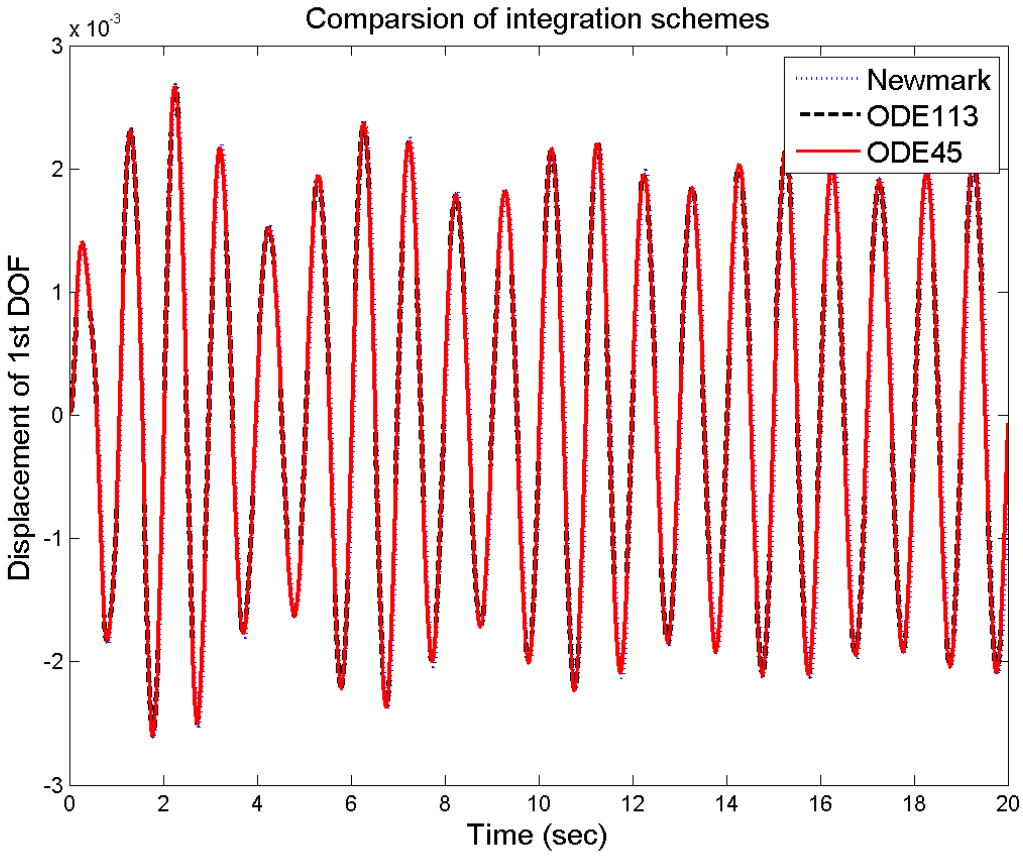

Figure 3-1. Validation of Newmark integration method by comparison of results with built-in MATLAB functions (ode113 and ode45).

Newmark type here is average constant acceleration, taking Alpha and Beta multiplier (α and β) as much as 0.5 and 0.25 respectively.

Result of least square method

Application of least square method in this study is obtaining unknown excitation forces which act on conjunct substructure, for this purpose all the DOF need to be observed on the substructure which is imposed to unknown excitation load. In this example, load is applied on first DOF and there is no force on other DOFs. Although this consideration will not be in contradiction to generality of the example. Therefore excitation forces in other DOFs need to converge to zero in all time steps.

Figure 3-2 and Figure 3-3 have shown the estimation of excitation force on first DOF for a sinusoidal and an arbitrary excitation. The result are presented after four hours of central processing unit (CPU) time.

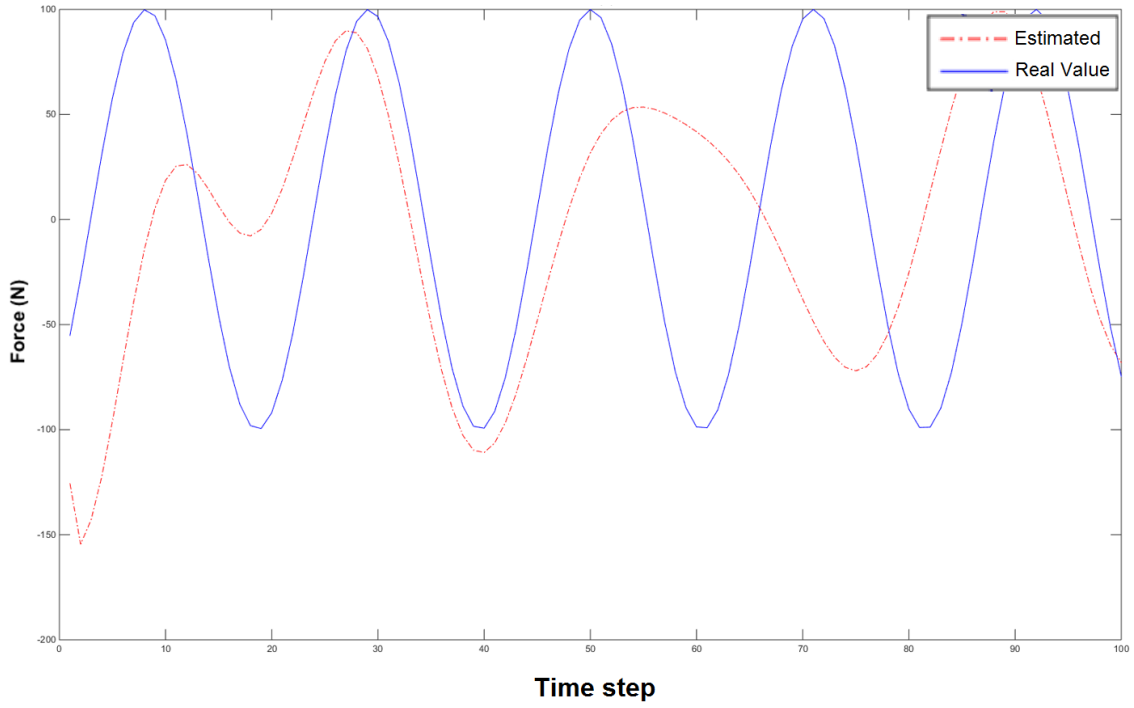

Figure 3-2. Estimation of a sinusoidal excitation force for 100 time steps.

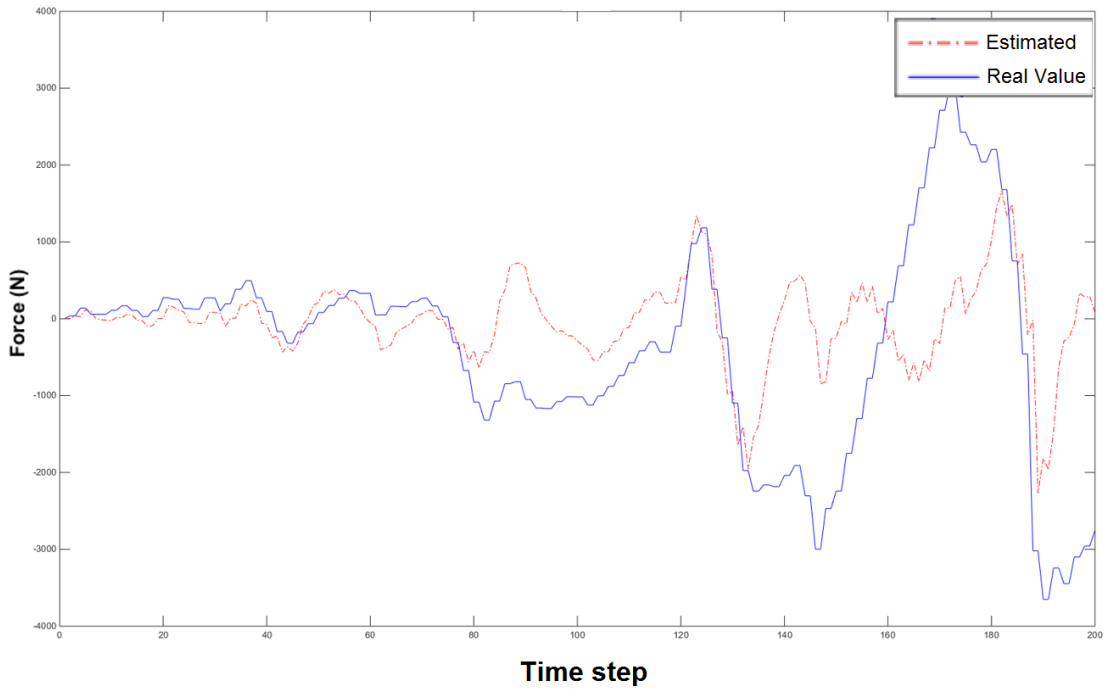

Figure 3-3. Estimation of an arbitrary excitation force for 100 time steps.

The convergence of the least square is not appropriate in reasonable time for presented time period, therefore this method is not robust and accurate enough in to be used in estimation. In Table 3-3 parameters of the system and result of estimation is presented.

Table 3-3. Least square method estimation for 4 DOF system with unknown force.

Coefficient	Estimated	Exact values
k_1	11144	8000
k_2	1728	4500
k_3	2103	3500
k_4	1988	3500
c_1	154	32
c_2	98	18
c_3	37	14
c_4	79	14

The displacement and velocities of all system DOF is not available in realistic situation. It is not feasible to obtain such data from model for all DOFs especially when rotational DOF

are under consideration. As result method is not logical to be applied for large systems. In practice, obtainable data are only accelerations and model displacement before excitation. Generally velocity in first step can be defined as zero, since system is assumed static before any loading applied on it.

3.2 Kalman estimator results for spring-mass-damper systems

Same 4 DOF structural as introduced in previous section is taken for Kalman estimator, as it illustrated on Figure 3-4, the excitation force is considered only on first DOF. Observation vector contains dynamic of system (one displacement, velocity or acceleration) for first DOF through all time steps, second DOF is considered as interface node.

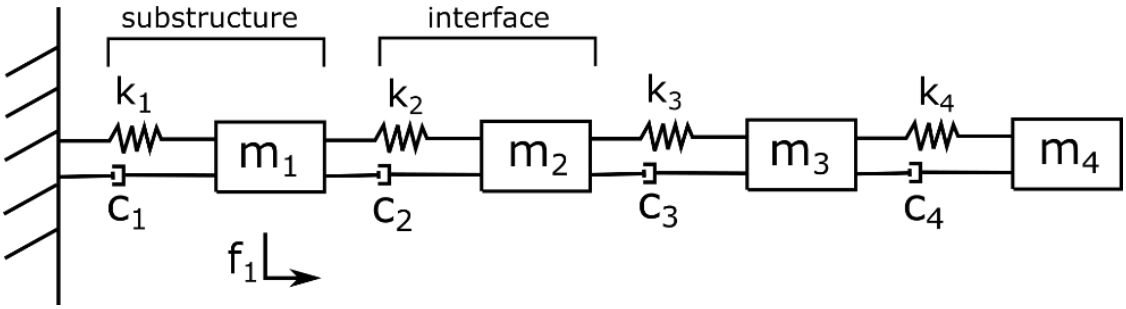

Figure 3-4. Spring-mass-damper structure with 4 DOF used for application of Kalman estimator.

In first step for initial covariance matrix, corresponding values for displacement and velocity are considered to be small, but the values of unknown parameter need to higher.
From stiffness and damping matrix we can write:

$$C_{11} = c_1 + c_2\,;\; K_{11} = k_1 + k_2\;;\; C_{12} = -c_2\;;\; K_{12} = -k_2\,;\;\; M_{11} = m_1 \qquad (3.2\text{-}1)$$

Where C_{11} shows first column entry in first row of damping matrix, K_{11} shows first column entry in first row of stiffness matrix and M_{11} presents first column entry in first row of mass matrix (C_{12} and K_{12} is the entry located in first row and second column). State space vector and its derivative in continuous form are as follows:

$$X = \begin{bmatrix} x_1 \\ \dot{x}_1 \\ C_{11}/M_{11} \\ K_{11}/M_{11} \\ K_{12}/M_{11} \\ C_{12}/M_{11} \end{bmatrix} = \begin{bmatrix} x_1 \\ x_2 \\ x_3 \\ x_4 \\ x_5 \\ x_6 \end{bmatrix} \qquad \dot{X} = \begin{bmatrix} \dot{x}_1 \\ \ddot{x}_1 \\ 0 \\ 0 \\ 0 \\ 0 \end{bmatrix} \tag{3.2-2}$$

$$\ddot{x}_1 = {M_{11}}^{-1}(f_1 - x_3x_2 - x_4x_1 - x_5x_2 - x_6x_2)$$

Where x_1 and $\dot{x}_1$ are first element of Space State vector and its first derivative with respect to time respectively. In same manner for x_2 to x_6 which are second to sixth row of vector X. Finally f_1 is imposed on first DOF. In this system the excitation is considered as known. In Table 3-4, the system coefficient are mentioned.

Table 3-4. Coefficient values for spring-mass-damper system in Figure 3-4.

DOF	Mass (kg)	Stiffness	Damping
1	20	10000	200
2	10	6000	100
3	10	3500	50
4	10	5000	100

Simulation time is considered as 2 second with 0.001 second time steps, and total of 10 global iterations. Noise pollution equal to 2.5 and 15 percent is imposed to observation vector in first and second set of results. Figure 3-5 is depicted original signal and adjacent polluted signal as part of observation vector.

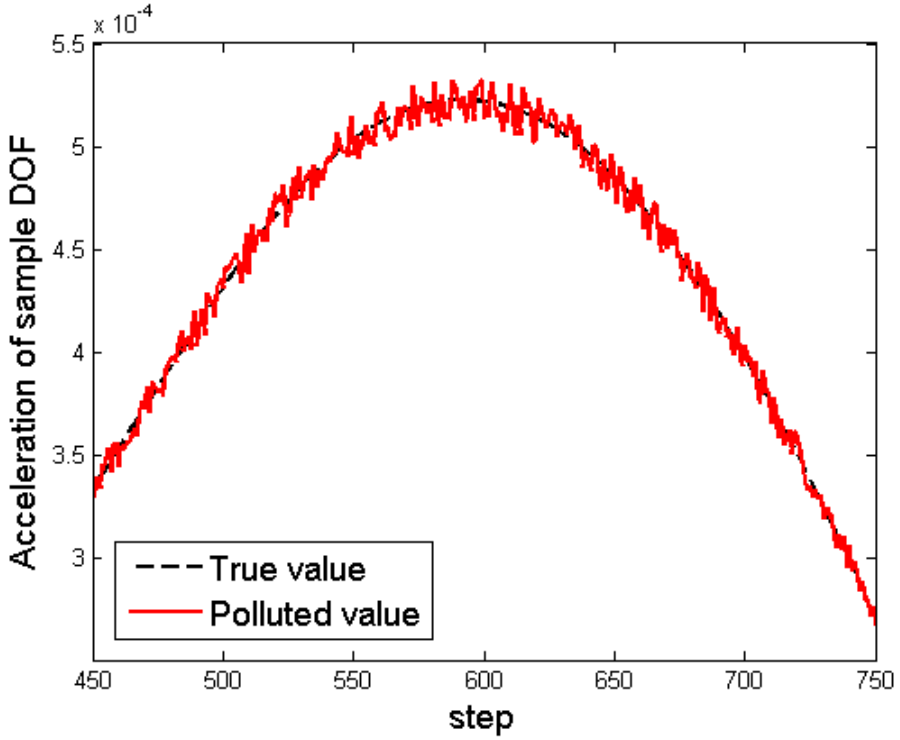

Figure 3-5. Noise pollution of the observation signal for sample DOF acceleration.

3.3 Effect of noise in convergence of Kalman estimator

Noise represents inaccuracy in observation, as all measurement methods are polluted with noise. Here to show effect of noise, two completely different ratios are considered for to simulate noise in recorded signal. First low noise result with 2.5 percent

Results with low noise (2.5%) with 100 as global weighting

Following figures have shown convergence of estimated parameters for the introduced system. As a proof of convergence displacement, velocity, or acceleration of the estimated system need to match simulated system. These results are depicted in Figure 3-6 and Figure 3-7, the red line shows the real value in the model, the black line is the estimated value through stages of global iteration.

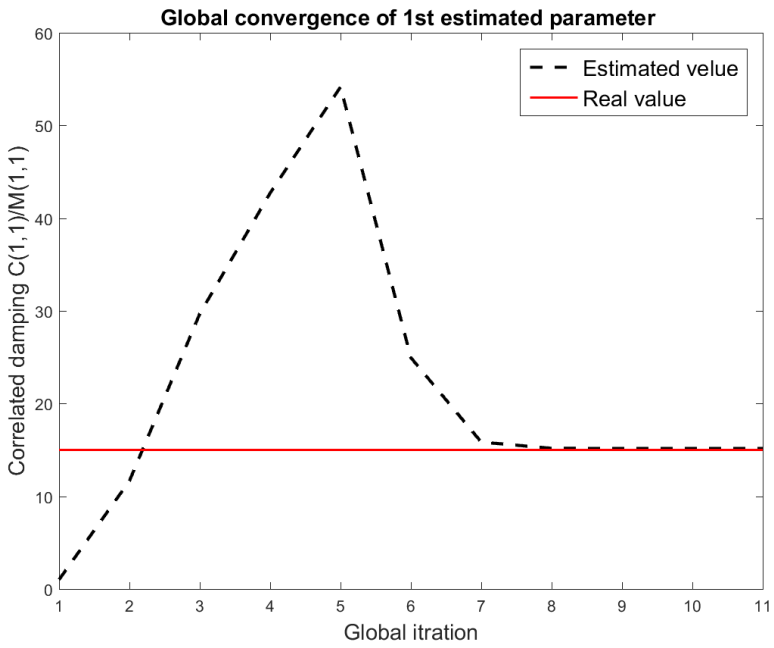

Figure 3-6. Convergence of damping coefficient for first DOFs (2.5% noise).

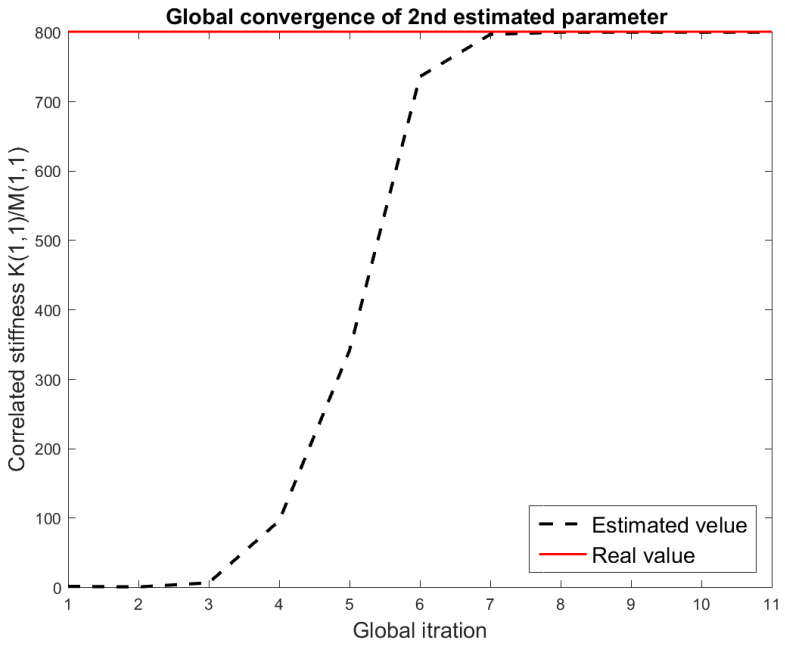

Figure 3-7. Convergence of stiffness coefficient for first DOFs (2.5% noise).

After several few start step the initial guess peak, in this time Kalman gain matrix will reach its maximum to correct the error accordingly. During early iterations, the estimated value may oscillate near the actual value. This oscillations is always accompanied and simultaneous with other parameters under estimation. In other words, estimated parameters

converge almost at same time, here around 8th steps of global iteration. In Figure 3-8 and Figure 3-9, convergence of two other coefficient are depicted.

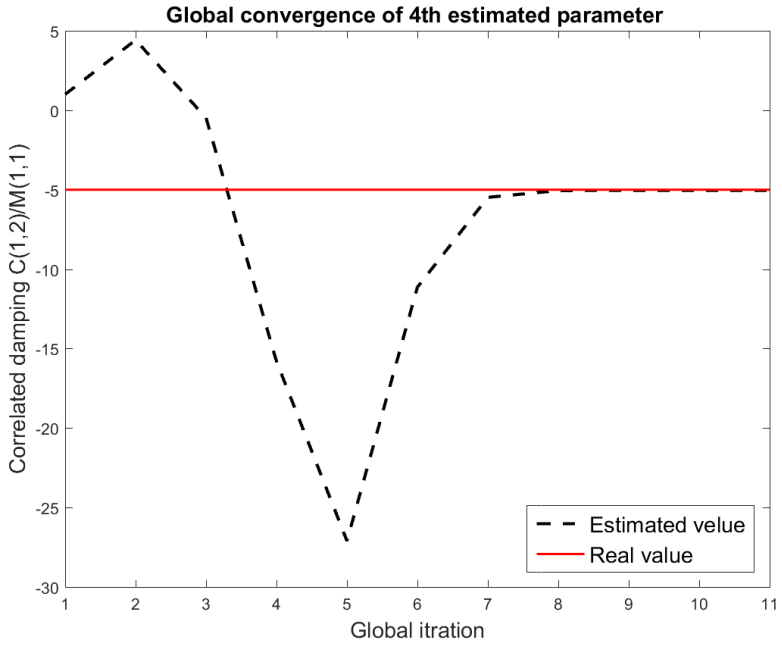

Figure 3-8. Convergence of damping coefficient for second DOFs (2.5% noise).

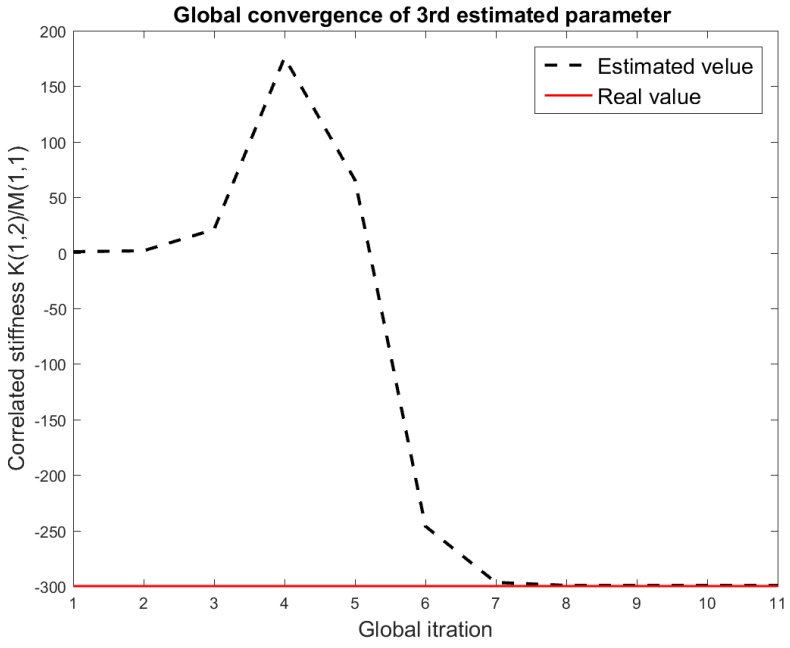

Figure 3-9. Convergence of stiffness coefficient for second DOFs (2.5% noise).

Results with high noise (15 percent) with 100 as global weighting

Effect of noise is present in following graphs, in Figure 3-10 to Figure 3-15. It can be noticed that final convergence was quite delayed cause of high noise. Also the amount of error in converged value stands higher.

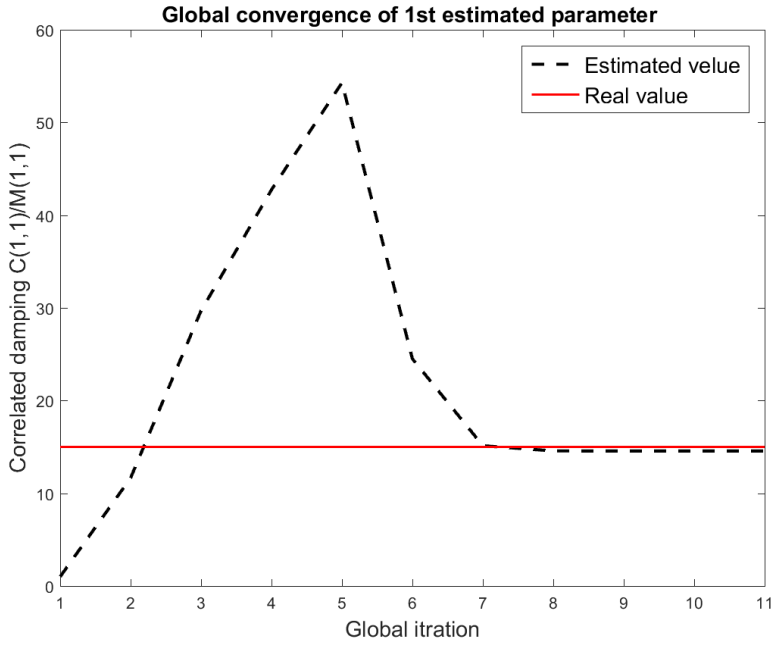

Figure 3-10. Convergence of damping coefficient for first DOFs (15% noise).

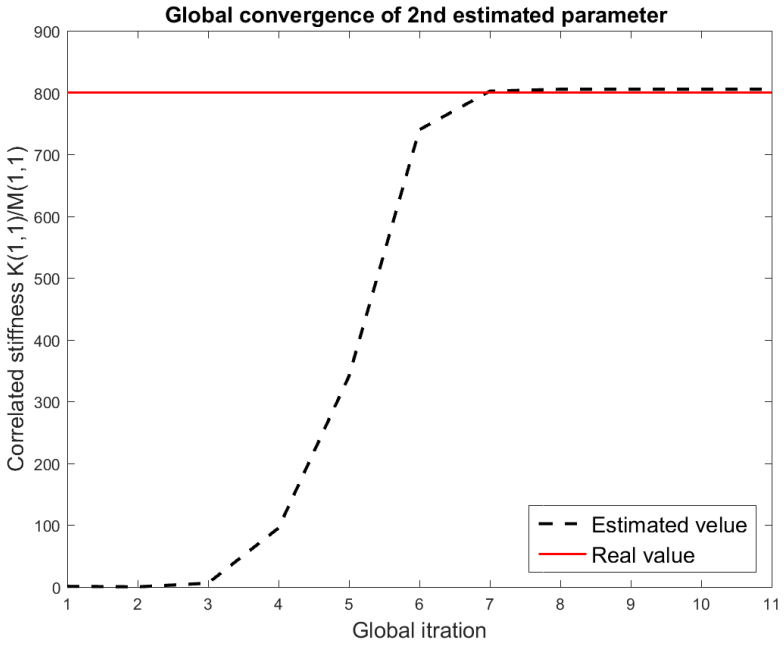

Figure 3-11. Convergence of stiffness coefficient for first DOFs (15% noise).

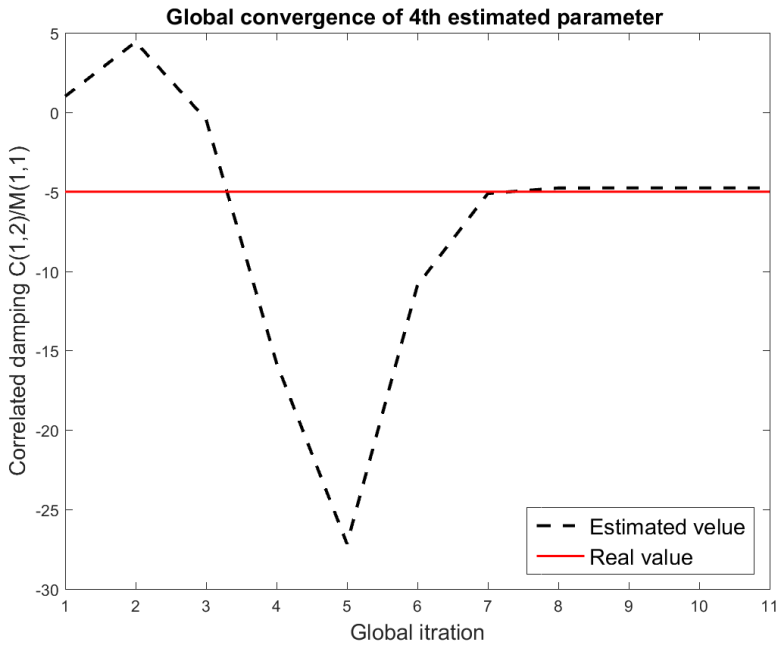

Figure 3-12. Convergence of stiffness coefficient for second DOFs (15% noise).

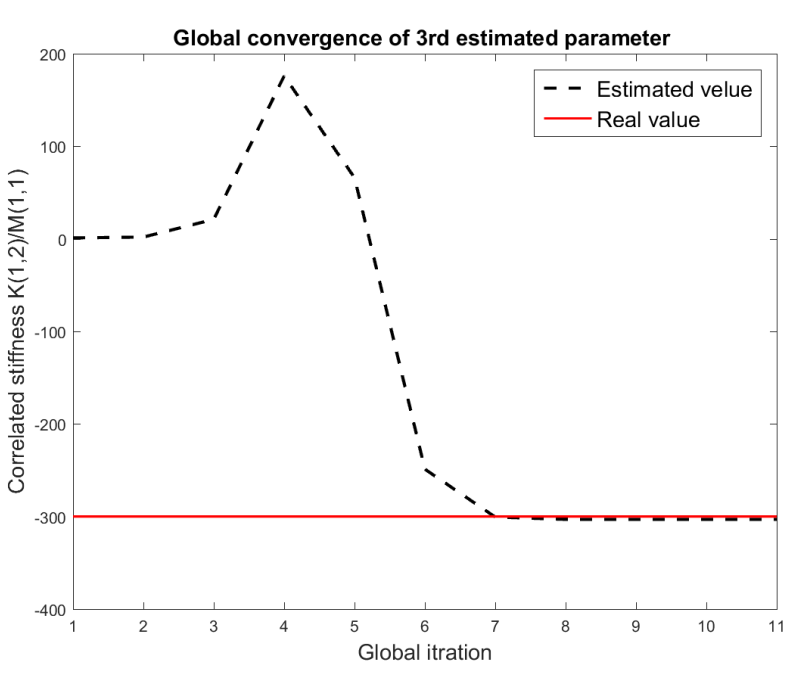

Figure 3-13. Convergence of damping coefficient for second DOFs (15% noise).

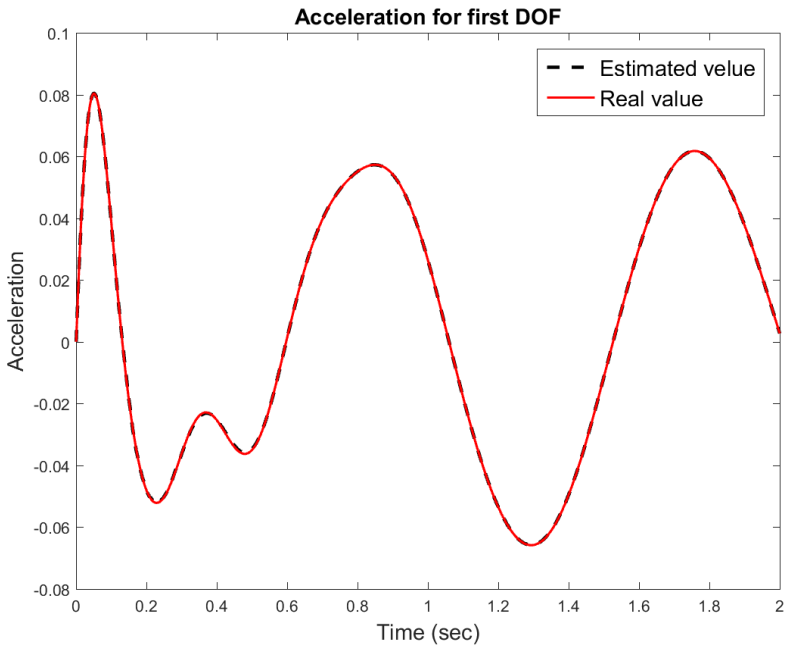

Figure 3-14. Convergence of system acceleration with 2.5% noise in last global loop.

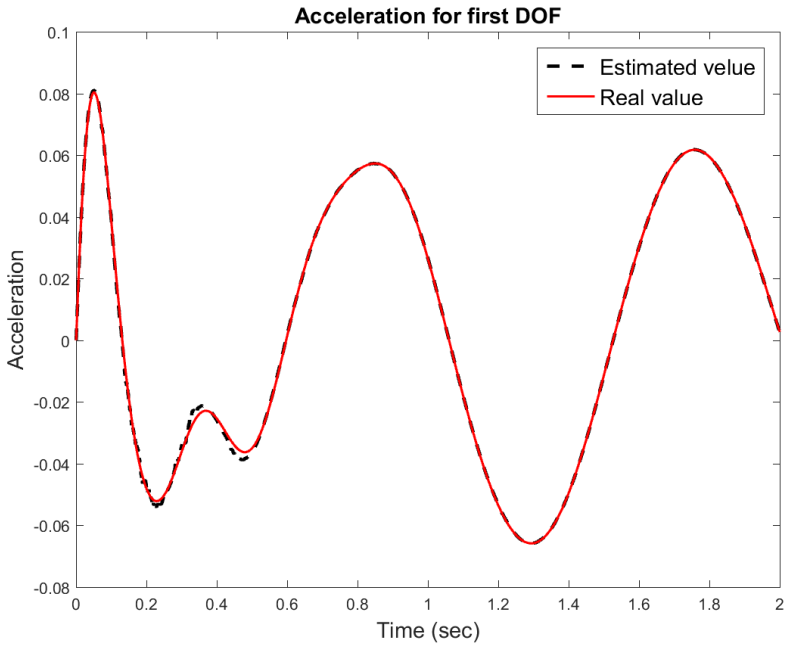

Figure 3-15. Convergence of system acceleration with 15% noise in last global loop.

Above mentioned Figure 3-14 and Figure 3-15 have compared acceleration in 1st DOF as a sample of system dynamic. It can be notice that the amount of error in steep changes is relatively high and estimation is not as exact as parameters that are estimated by lower noise in presented model of the system.

3.4 Effect of global weighting in estimation convergence

Result of estimation are presented in following table, in two cases. In first case, results are obtained by smaller global weighting. The error in estimated values with relatively smaller weighting is less, in price of slower estimation convergence.

Summary of results after 10 global iteration are presented in Table 3-5, while observation is imposed of 15 percent white noise. This result are computed with 100 weighting factor in start of each global iteration.

Table 3-5. Estimation of part of stiffness and damping matrix for 4 DOF system by Kalman two-stage estimator with different global weight iteration.

Coefficient	Initial guess	Estimated value (Weight=10^2)	Estimated value (Weight=10^5)	Exact coefficient
K_{11}/M_{11}	1	787.0	810	800
K_{12}/M_{11}	1	-291.8	-307.3	-300
C_{11}/M_{11}	1	15.39	14.09	15.0
C_{12}/M_{11}	1	-5.02	-4.38	-5.00

Also it is noteworthy to mention, error in damping coefficient are relatively high, but considering small effect of damping in comparison to stiffness coefficient in system dynamics, these values are acceptable. Higher accuracy can be achieved with finer time step size and better ratio in first initial guess of coefficients.

4 APPLICATION SUBSTRUCTURE DAMAGE DETECTION ON SYSTEMS ATTACHED TO BEAM-LIKE ELEMENTS

In this section implementation of the Kalman estimator on beam elements are introduced. For the sake of simplicity, the blade of Turbine is modelled as a beam substructure in this chapter. The whole system though is not necessarily needed to be made with beam elements, any other element type might be considered.

4.1 Beam elements

Main difference between beam elements and previously introduced spring-damping-mass system is number of DOFs in each node. A beam can resist bending and transverse forces. If axial force in beam modelling is neglected, every node of the beam in a two-dimensional space has 2 DOFs, for translational displacement (here vertically) and rotational displacement.

Curvature of a beam can be defined by writing displacement of the beam in two-dimensional coordinates as [33]:

$$\nu = a_1 + a_2 u + a_3 u^2 + a_4 u^3 \tag{4.1-1}$$

When ν as translational displacement of the beam, is an equation based on u which is horizontal position on the beam and a_i as curvature parameters, estimate real physical shape by:

$$\nu = [z_1 + z_2 + z_3 + z_4] \begin{bmatrix} \nu_1 \\ \theta_1 \\ \nu_2 \\ \theta_2 \end{bmatrix} = \mathbf{Z} \begin{bmatrix} \nu_1 \\ \theta_1 \\ \nu_2 \\ \theta_2 \end{bmatrix} \tag{4.1-2}$$

Where $\mathbf{Z}$ is shape function and each z_i presents special deflection shape. Considering two nodes on an element, ν_1 and ν_2 are translational displacement of node 1 and 2. Then θ_1 and θ_2 are rotational displacements respectively (Generally ν and θ are used to show

translational and rotational displacements respectively). The beam deflection curves which represents how strain energy is stored can be written as:

$$\frac{\partial^2 \mathrm{v}}{\partial \mathrm{u}^2} = \left[\frac{\partial^2}{\partial u^2}\mathbf{Z}\right]\begin{bmatrix}\mathrm{v}_1\\ \theta_1\\ \mathrm{v}_2\\ \theta_2\end{bmatrix} \tag{4.1-3}$$

Then the strain-displacement matrix is represented by **B** as [34]:

$$\mathbf{B} = [-\frac{6}{l^2}+\frac{12u}{l^3} \quad -\frac{4}{l}+\frac{6u}{l^2} \quad \frac{6}{l^2}-\frac{12u}{l^3} \quad -\frac{2}{l}+\frac{6u}{l^2}] \tag{4.1-4}$$

Where *l* is length of the element, and **K** as stiffness matrix is integrated from strain energy of the elements as [33]:

$$\mathbf{K} = \frac{\mathrm{EI}_x}{l^3}\begin{bmatrix}12 & 6l & -12 & 6l\\ 6l & 4l^2 & -6l & 2l^2\\ -12 & -6l & 12 & -6l\\ 6l & 2l^2 & -6l & 4l^2\end{bmatrix} \tag{4.1-5}$$

Where E is modulus of Elasticity and I_x is moment of inertia. Mass matrix **M** for the beam can be derived from integration of shape function in volume of the beam as:

$$\mathbf{M} = \begin{bmatrix}\frac{13m}{35} & \frac{11ml}{210} & \frac{9m}{70} & -\frac{13ml}{420}\\ \frac{11ml}{210} & \frac{ml^2}{105} & -\frac{13ml}{420} & -\frac{ml^2}{140}\\ \frac{9m}{70} & \frac{13ml}{420} & \frac{13m}{35} & -\frac{11ml}{210}\\ -\frac{13ml}{420} & -\frac{ml^2}{140} & -\frac{11ml}{210} & \frac{ml^2}{105}\end{bmatrix} \tag{4.1-6}$$

Which have the m as the mass of the element. By substituting m as multiplication of density, cross section area and length, one can write diagonal estimation of mass matrix, neglecting coupling effect of other DOFs inertias [16]:

$$\mathbf{M} = \begin{bmatrix} \frac{\rho \mathrm{A} l}{2} & 0 & 0 & 0 \\ 0 & \rho\left(\frac{l^3}{24} + \frac{\mathrm{I}_x l}{2\mathrm{A}}\right) & 0 & 0 \\ 0 & 0 & \frac{\rho \mathrm{A} l}{2} & 0 \\ 0 & 0 & 0 & \rho\left(\frac{l^3}{24} + \frac{\mathrm{I}_x l}{2\mathrm{A}}\right) \end{bmatrix} \tag{4.1-7}$$

Where ρ and A are density and cross section area respectively. While equation (4.1-6) is known as consistent mass matrix, assume that mass of the element is distributed uniformly through beam volume, equation (4.1-7) as lumped sum mass matrix, is simplifying mass to a diagonal estimation. Computational effort for iteration based on Kalman estimator will significantly reduce with lumped mass model of the beam. This approach is applied on a multi degree of free (MDOF) in following section.

4.2 MDOF Beam identification with incomplete observation and diagonal mass

In industrial applications, linear sensors are less complicated, smaller and cheaper than angular sensors [35]. Therefore it is more efficient to consider observations only for translational accelerations [27]. But the model of the structure will not remain observable if all stiffness matrix element considered as independent variable like spring-mass-damper model. The solution to mentioned problem is discussed in following part.

Estimation of the parameter for a 4 DOFs beam

To address issue of non-observability of Kalman estimator with only displacement observation, defining independent variable is crucial. In this way, matrix elements need to be defined separately, and with help of a correlated coefficient. This coefficient introduces normal stiffness matrix with a multiplication of a scalar and a matrix. So it is assumed that every degradation will effect rotational and linear stiffness with same correlation. It shall be noticed that this multiplier is totally arbitrary, but will be considered in same way for all elements of the system. A beam structure is shown in Figure 4-1.

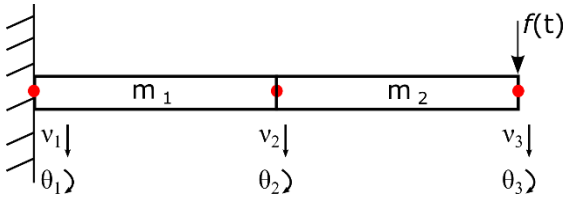

Figure 4-1. Beam model with two elements and 4 DOFs which is fixed in one end.

The beam is presented with 2 elements and one external excitation load is shown, the load is only consist of one transversal arbitrary force. Observation vector is not consist of angular DOFs, but one linear acceleration on each element. Figure 4-2 have illustrated the excitation for through the time.

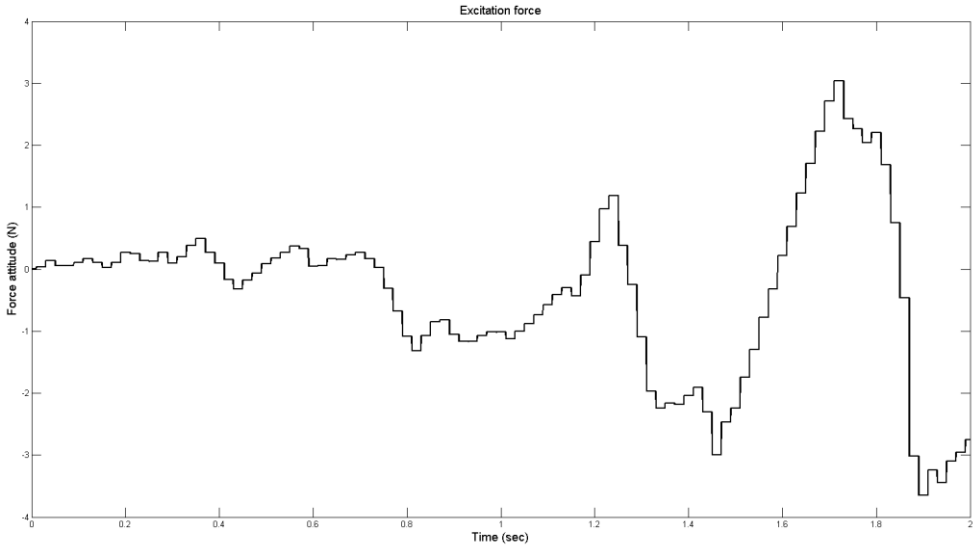

Figure 4-2. Arbitrary applied excitation force on the beam structure during 2 seconds time period.

The result of estimation in last loop of global iteration are shown for part of system dynamic in following figures. In addition convergence for acceleration of 1st DOF through global iteration 1 to 10 is depicted in the appendix. In Figure 4-3 and Figure 4-4 response of the system for first and third DOF is investigated in concern of acceleration.

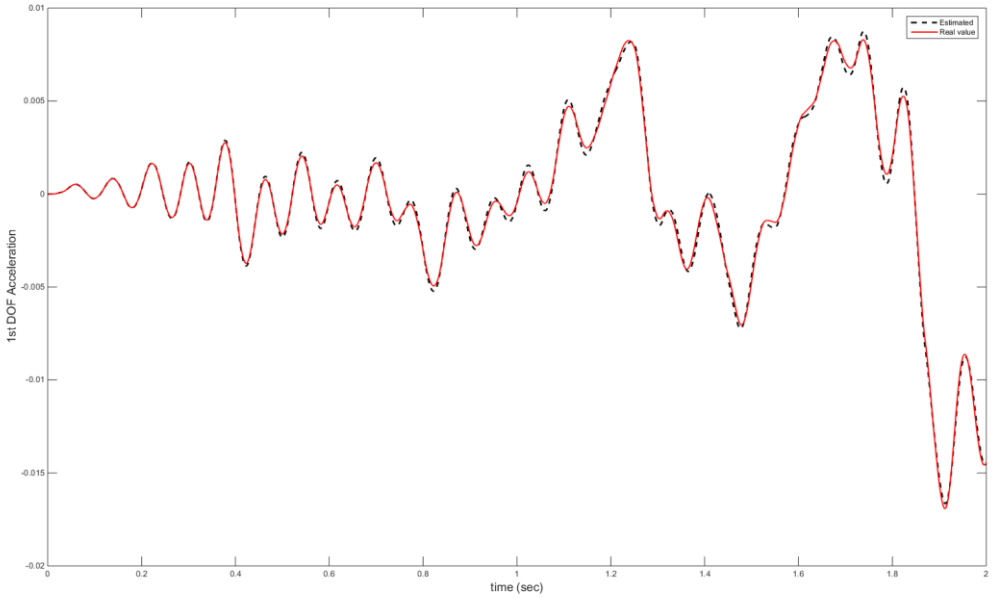

Figure 4-3. Estimation of 1st DOF acceleration in last global loop of iteration.

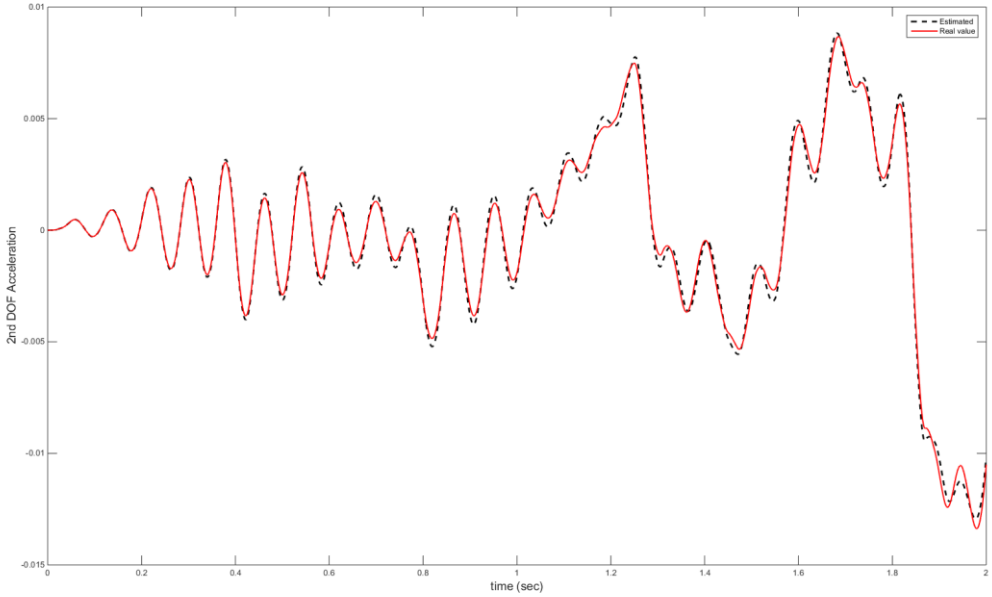

Figure 4-4. Estimation of 3rd DOF acceleration in last global loop of iteration.

As it can be noticed from figures, when there is a sharp change is acceleration, estimator will encounter larger errors. This can be compensated with smaller time step, when consideration is taken for reachable accuracy via demanded computational time. In Figure 4-5 velocity of the third DOF is shown.

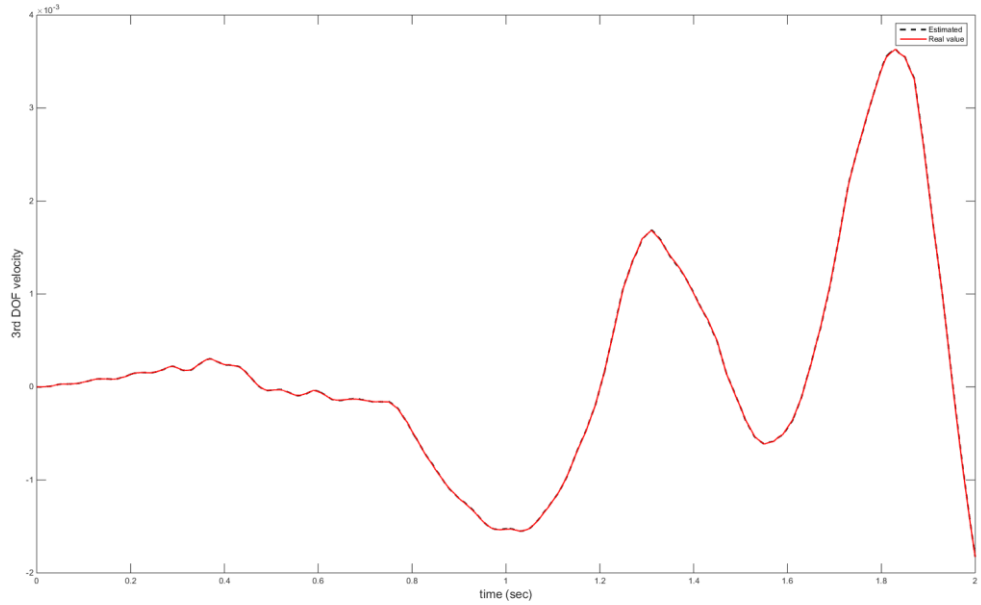

Figure 4-5. Estimation of 3rd DOF velocity in last global loop of iteration.

Estimated rotation for end of the beam on 4th DOF of the system is depicted on Figure 4-6, which fits the real value of the model. System dynamics obviously fits the graphs from simulation when there is no considerable discrepancy between expected values and identified values. Same behaviour is seen in Figure 4-7 and Figure 4-8.

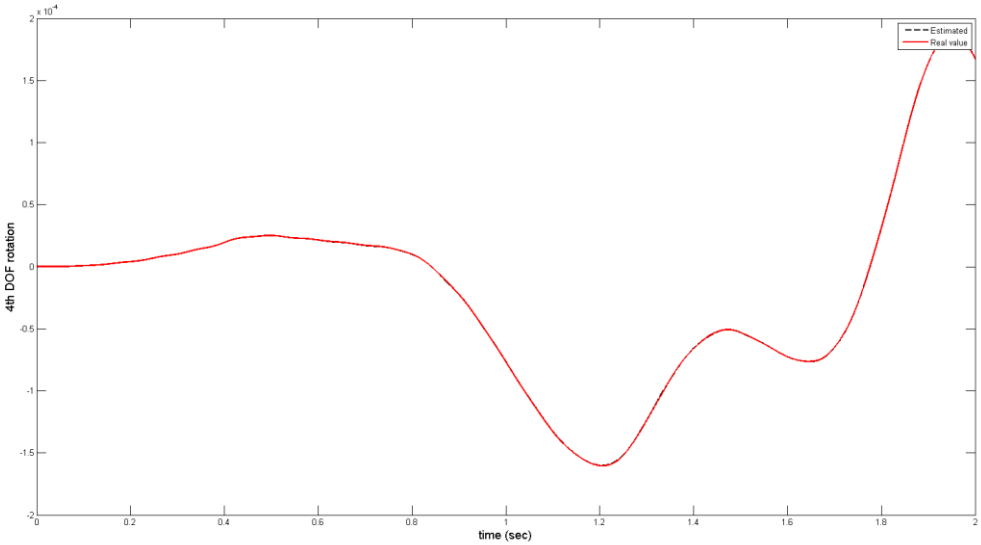

Figure 4-6. Estimation of 4th DOF rotation in last global iteration.

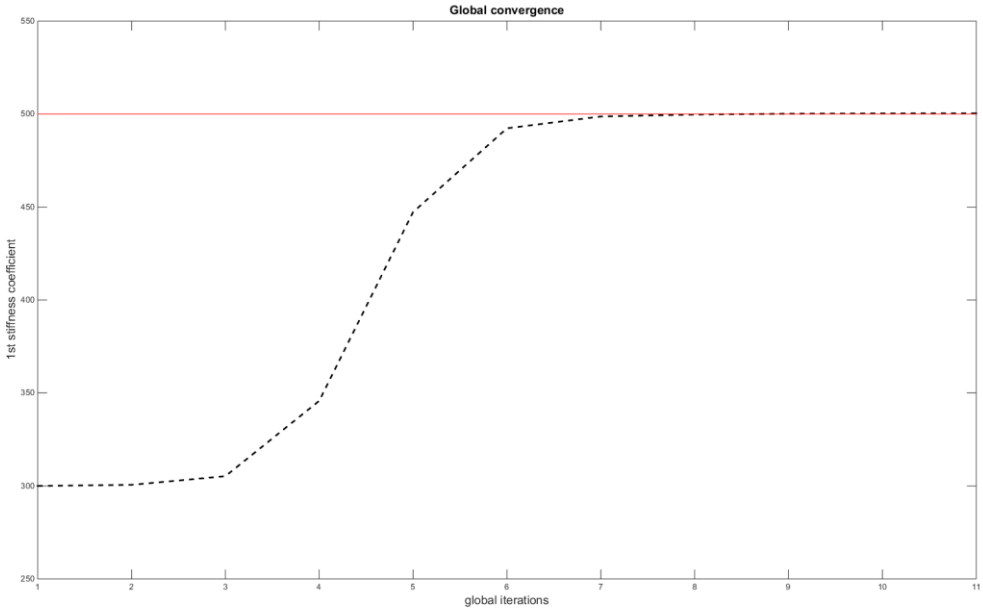

Figure 4-7. Convergence of first stiffness coefficient in global iteration.

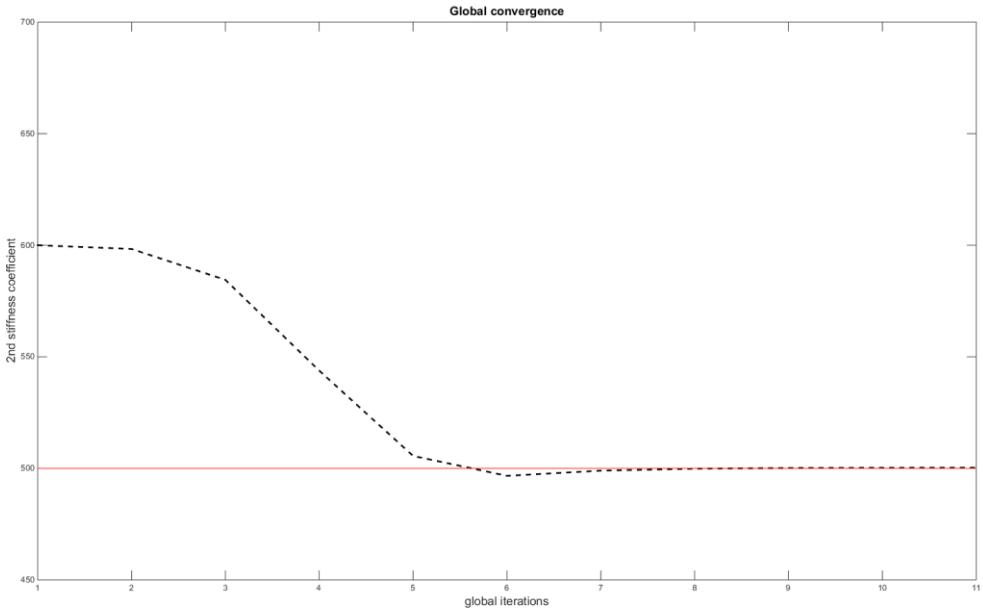

Figure 4-8. Convergence of second stiffness coefficient in global iteration.

System parameters for the beam model are estimated and illustrated in Table 4-1. Mass of the system is taken as noun, and initial values of the model are taken with large difference in comparison with real values. Results are obtained after 10 global iteration, when each global iteration has 20000 time steps (10^{-4} sec.) a simulation period.

Table 4-1. Estimated stiffness correlations for beam with two elements.

Parameter	Initial guess	Real value	Estimated
Stiffness correlation factor of k_1	300	500	500.382
Stiffness correlation factor of k_2	600	500	500.280

Accuracy of result can be increased, in cost of higher computational power, by finer time steps. It shall be noted that higher number of global iteration will not necessarily lead to better accuracy when global iteration is already converged.

4.3 Noise pollution of the observations

The noise which is employed to pollute the observation vector is normal distributed white noise with no bias, the noise function as default is correlated with magnitude of measurements, although this assumption can raise questions regarding effect of different noise construction in calculations. Therefore in several trial different noise functions is added (as an example MATLAB functions randn and rand) and no observable change is seen. The Kalman estimator algorithm have shown good stability in presence of noise, the effect of different noise amplitudes are presented in following sections.

4.4 System identification with unknown forces and non-diagonal mass matrix

During the damage detection process, cause of system boundary condition and numerous DOFs, often the load which act on the substructure is unknown. Also there are many concerns about system excitation. Although diagonal mass matrix which is used in recent literatures have simplified the simulation and decreased the computational effort, but model accuracy can be highly influenced in these systems. Therefore in this subchapter parameter estimation with complete mass matrix and unknown forces is investigated.

The force estimation process is performed based on concept of least square method, although special consideration for the convergence is required. The Kalman estimator inherently use a gain value (Kalman gain) for improvement of the estimation in each global iteration, which is in correlation with initial covariance matrix of the initial guess in each stage of global iteration. The initial guess vector and its correlated initial covariance matrix are updating in start of each global iteration, which affecting all internal iterations of Kalman estimator belong to that specific global loop.

Obtaining converged results in reasonable time is only possible with help global weighting factor, which is multiplied to initial covariance matrix in start of each global iteration. This weighting naturally can make Kalman oscillations in calculation stages, leading to divergence of whole estimation. In other hand without such weighting, results are diverged after numerous numbers of estimation with inappropriate initial guess. As initial guess need to remain unconditional and free of assumption for a robust method, use of weighting is normally required when unknown forces are involved. In Figure 4-9 a beam is schematically connected to an unknown structure.

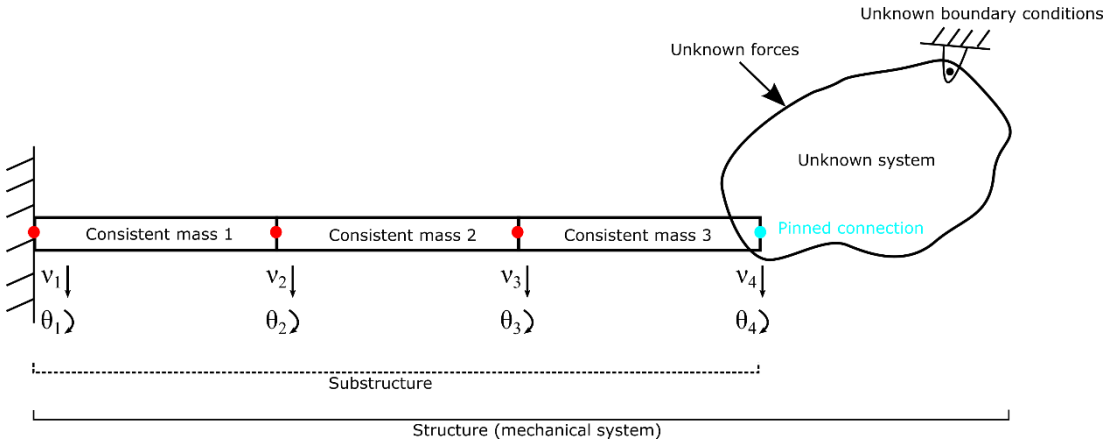

Figure 4-9. Substructured beam under unknown forces.

In estimation with unknown forces, when the load is not good estimation of the actual force value through simulation steps, this oscillation will easily lead to divergence estimated parameters. This diverged estimated parameter will again make an improper guess for the estimated force in following global iteration, as the force estimation loop is one loop delayed from parameter estimation. In this way, whole estimator is diverged without possible successful results.

The solution is possible by help of variable weighting of the Kalman. In variable weighting, early global loops will improve the force estimation. The small weighting factor keep the initial guess of system parameters without change, meanwhile the force estimation process forms a good estimation through time steps. It is noteworthy to mention minimum size of unknown variable force is as large as number of time steps but not same as integration time steps. After primitive estimation of the force, the weighting factor increased in several stages to speed up the divergence process.

The most important aspect in start of the estimation is proper detection of the force, in Figure 4-10 first estimation of the load is shown. In this stage, the system parameters are not close to real values. To show robustness of proposed method, for first guess is chosen with a large difference with real value, these parameter are presented in Table 4-2.

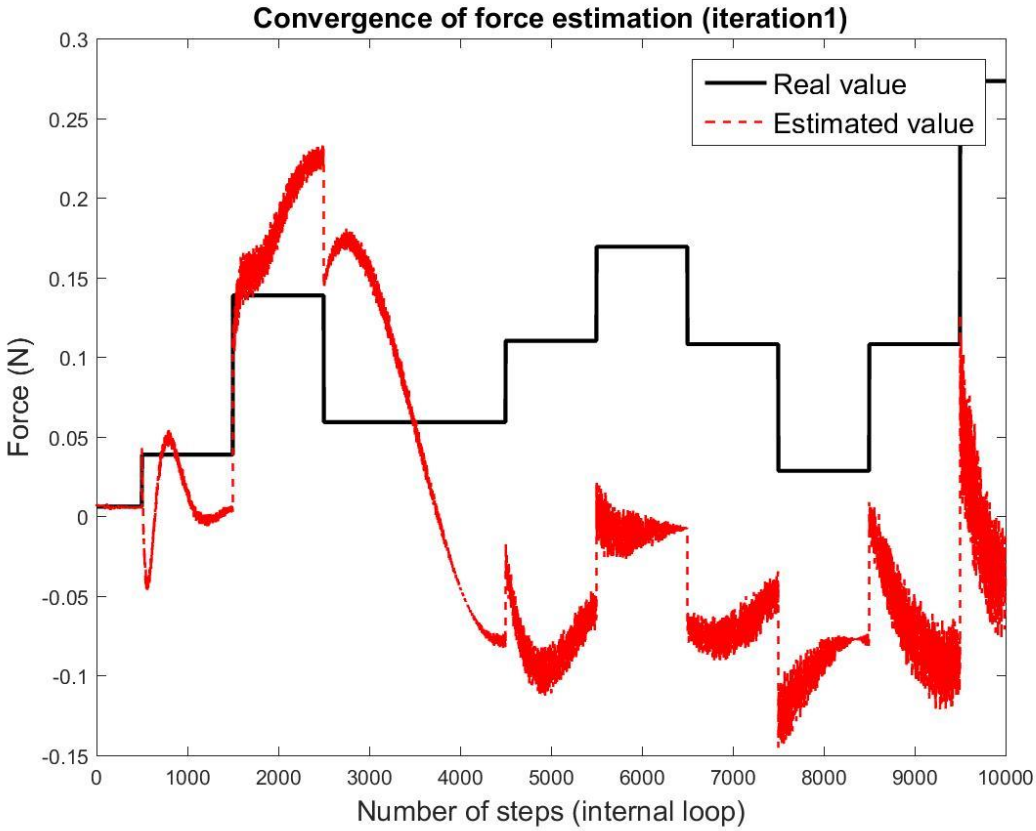

Figure 4-10. Convergence of the estimated force in after first iteration.

Table 4-2. Initial guess for concerned beam substructure.

Parameter	Initial guess	Real value
Stiffness correlation factor of k_1	25000	50000
Stiffness correlation factor of k_2	100000	50000
Stiffness correlation factor of k_3	58000	50000

After several initial iteration, force estimation reach the close to real value, in Figure 4-11 this trend is shown. It is noteworthy to notice in this stage of estimation, parameters are not good approximation of actual values.

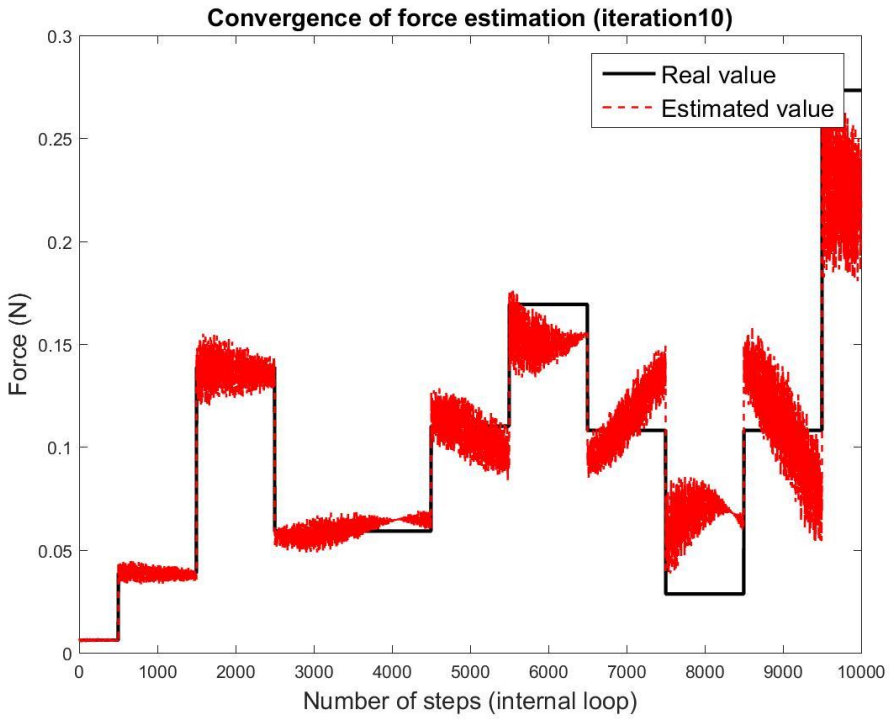

Figure 4-11. Convergence of the estimated force in after 10th iteration.

This trend is continued by several early iterations, till unknown force will not change in comparison of the previous iteration. Here in the experiment the extract acting force which is used for simulation of the substructure is drawn alongside of the estimated force. It is obviously can be observed that when the force estimation is not changing anymore through the loops, the estimated force is closely converged to real excitation force. It shall noticed that the force is only used in the graph presented from but not for estimation iteration, as it is initially considered as unknown. Unknown force in this estimation have 10000 independent unknown variables, same number as time steps, which is needed to be estimated.

Convergence of system parameters are shown in Figure 4-12, the early iterations from 1 to 26 are not embarking a change in initial guessed values. As an example, the k_1 correlated value is 27450 (comparing to 25000 in initial guess) and k_2 is 90935 which is almost 4 times more than correct stiffness. Obviously main convergence of the parameters is happened after 26th iteration.

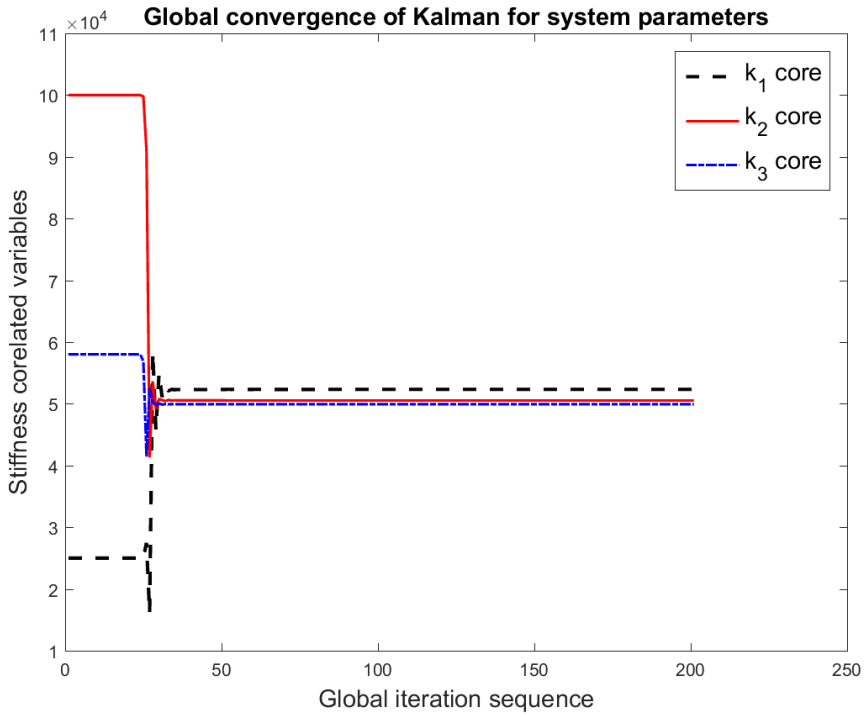

Figure 4-12. Convergence of correlated stiffness values through global iterations.

Steps of global iteration, the variable weighing is shown in Table 4-3. As a general rule based on presented result, the weighting need to be delayed till there is no big change in the estimated force, then on next stage weighting can be applied for estimation of the parameters.

Table 4-3. Variable weighting of the global iteration through initial covariance matrix.

Global iteration	Global weighting on initial covariance matrix
Loop 1 to 19	No weighting
Loop 20 to 50	100
Loop 50 to 200	1000

Sample result of convergence in substructure dynamics is shown is presented through Figure 4-13 to Figure 4-18. The estimated results are good estimation of the real values. The amount of error is almost negligible and error is mainly is result of numerical inaccuracy which can be improved by smaller time steps.

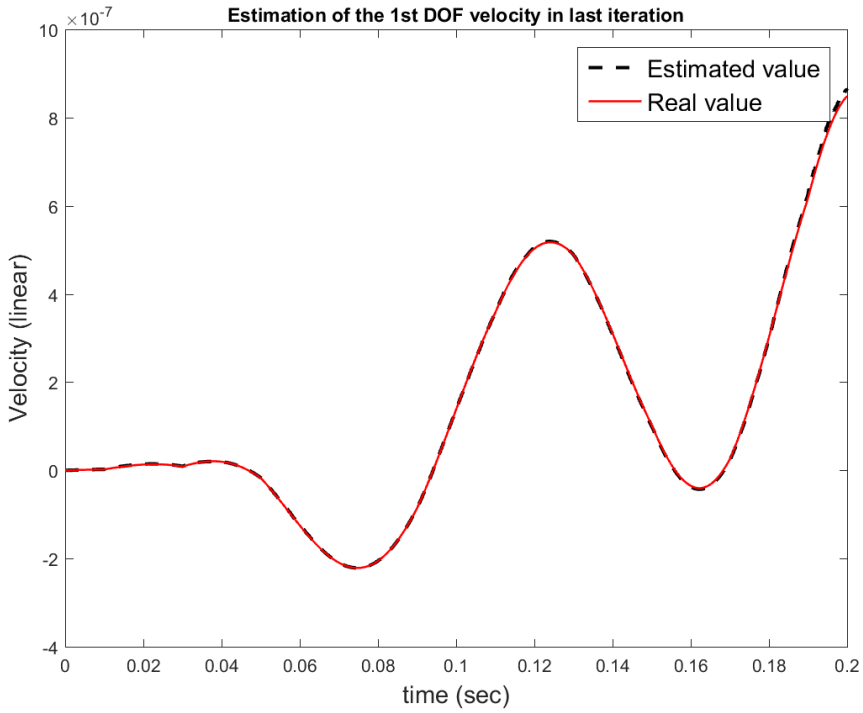

Figure 4-13. Estimation of 1st DOF velocity in comparison to real value.

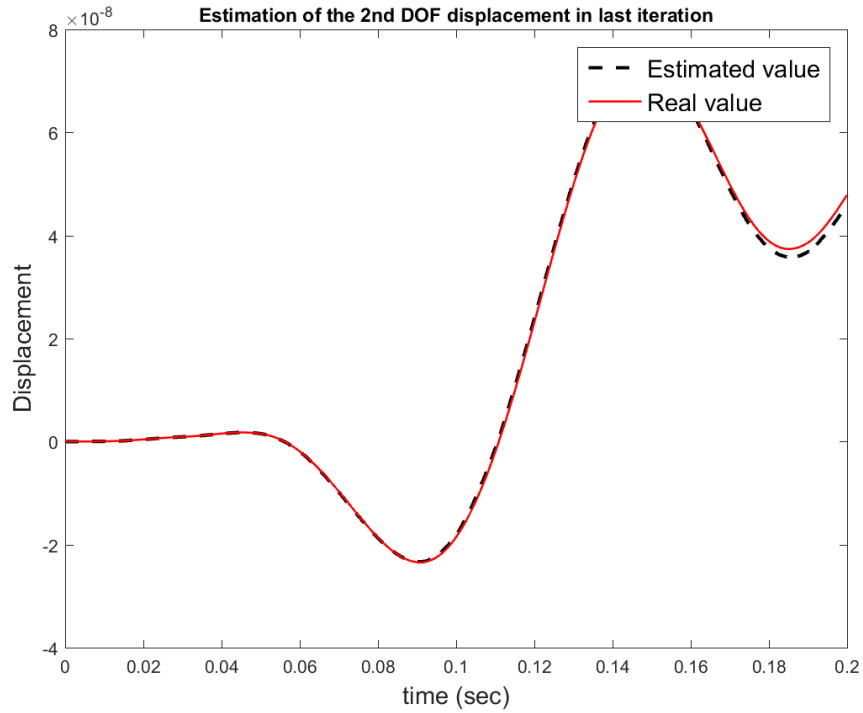

Figure 4-14. Estimation of 2nd DOF displacement in comparison to real value.

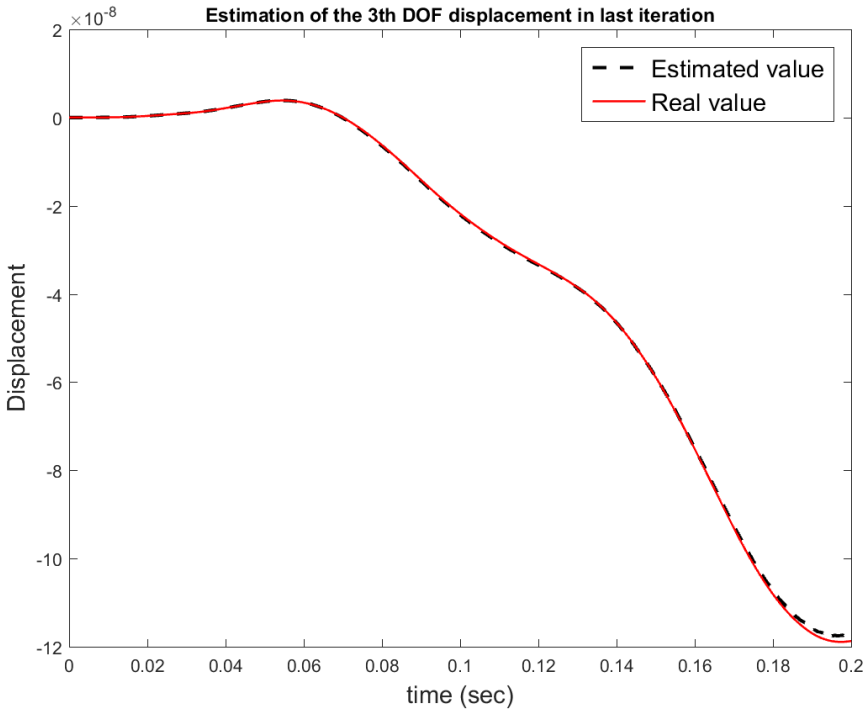

Figure 4-15. Estimation of 3rd DOF displacement in comparison to real value.

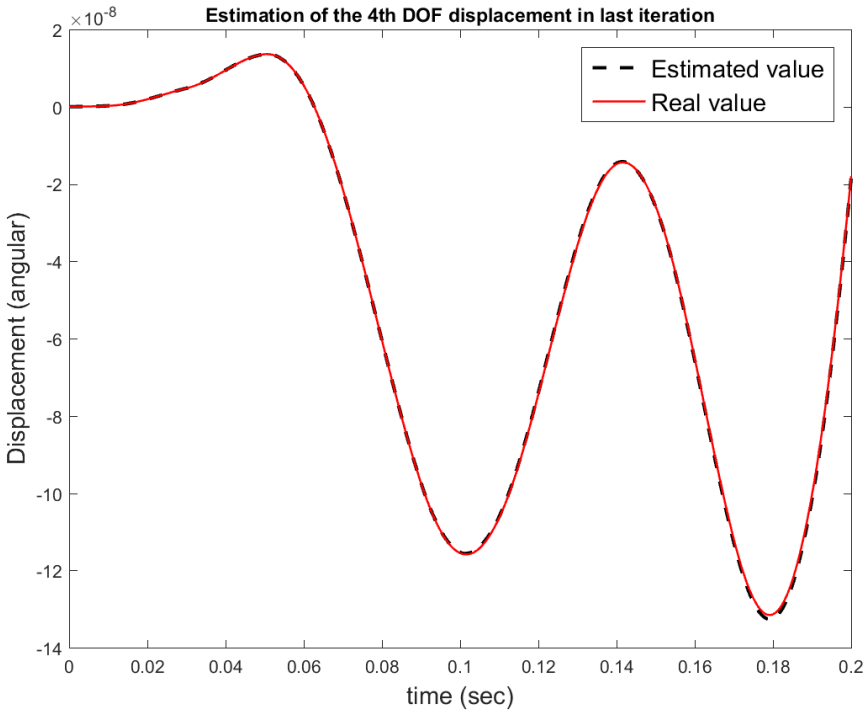

Figure 4-16. Estimation of 4th DOF velocity in comparison to real value.

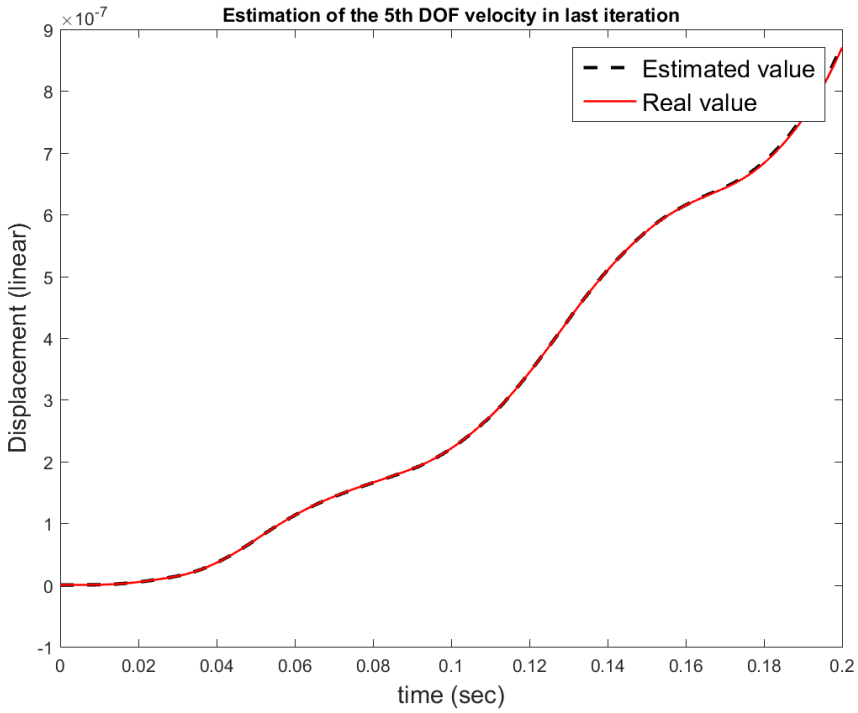

Figure 4-17. Estimation of 5th DOF displacement in comparison to real value.

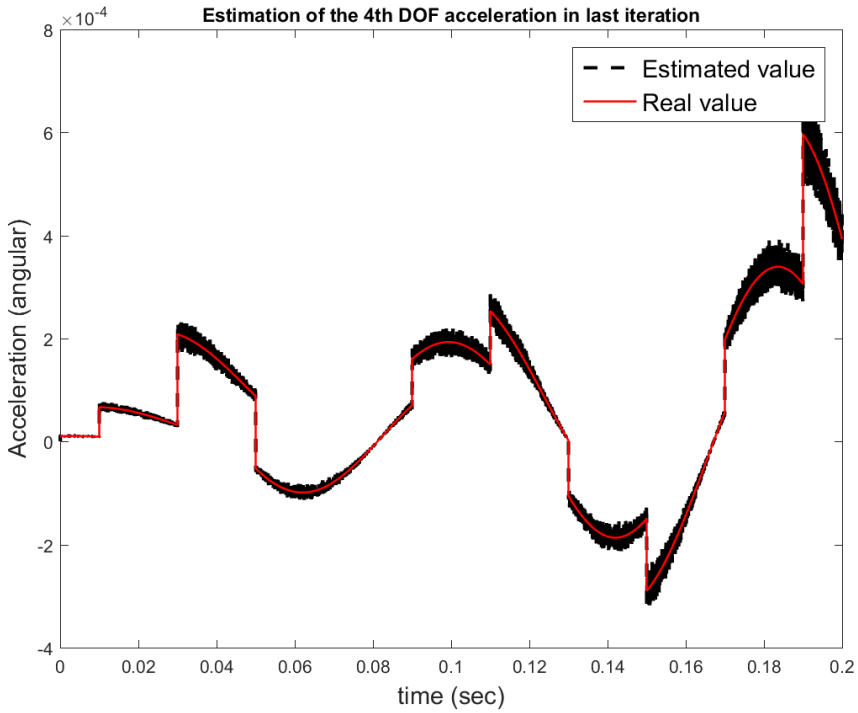

Figure 4-18. Estimation of 4th DOF accelration in comparison to real value.

In Table 4-4 final result of the model estimation is presented, 30th iteration as sample is compared to final stage of the estimation to investigate the convergence behaviour.

Table 4-4. Final results and relative error after convergence.

Parameter	Real value	Converged value at 30^{th} iteration	Converged value at 200^{th} iteration	Error percentage
Stiffness correlation factor of k_1	50000	50732	51989	3.978 %
Stiffness correlation factor of k_2	50000	50743	50660	1.320 %
Stiffness correlation factor of k_3	50000	49850	49922	0.156 %

Highest amount of error belongs to first correlated value, but as seen in previous estimations, this error can be reduced by finer time step. This estimation carried out with 0.02 millisecond step size, in presence 5 percent noise and for 10000 time steps. Meanwhile different step size is considered for Newmark integration, so the simulation had 4 times smaller time step.

5 APPLICATION OF THE METHOD FOR WIND TURBINE BLADE

Damage detection techniques based on substructuring can be applied in parallel or independent from non-destructive test of mechanical systems. Once measurement is done with help of accelerometer sensors, gathered data is used to reveal possible fault considering its location and intensity. This chapter explain application of the presented method on a wind turbine blade as test bench.

5.1 System identification for blade of a turbine

A wind turbine rotor is considered as test bench of method. AMPAIR 600 have previously chosen as a test bed for several substructuring based studies [36–38]. A complete CATIA model is presented in Figure 5-1. The rotor is consist of three tapered blades which are joined to hub in the center, assembled on an aluminium pole as tower. Total weight of the system is 114 Kg which is mainly result of its support pole and baseplate. The height of from baseplate to generator is 185 cm and nominal generated power around 600 watts. [39]

Figure 5-1. Complete test bench of Wind Turbine modelled with help of CATIA.

Blade are made of glass reinforced polyester material. Total rotor diameter is 1700 mm [40] and though for simplification they considered to be made of one isotropic material. Shape of one blade is depicted in Figure 5-2.

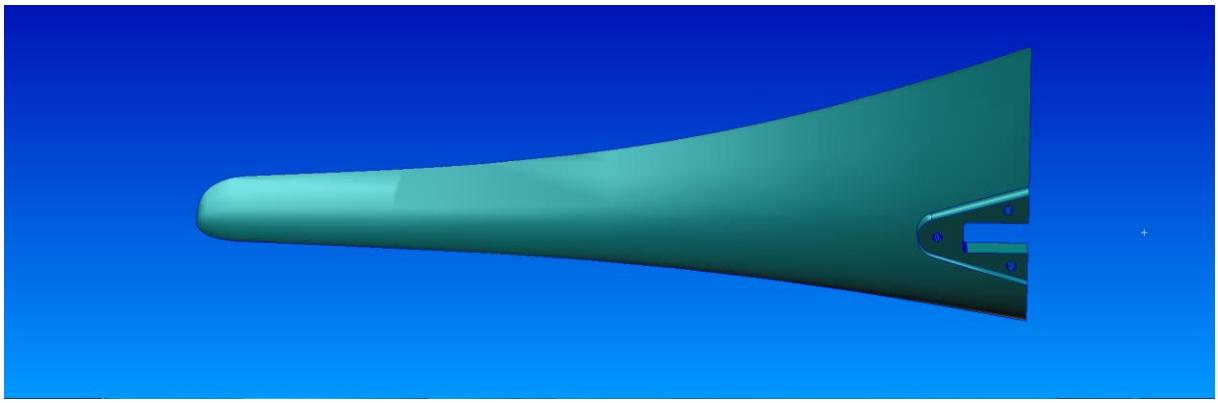

Figure 5-2. Blade of the Wind Turbine which used as representative of a mechanical system.

Since the geometry of the blade is not changing in wide range, it can be represented with plate elements, obviously thickness of the plate is smaller than other dimensions including width and length.

5.2 Characteristics of Nastran CQUAD4 plate element

Plate elements have the potential to be representative for the realistic simulation of the turbine blade. They can carry different loads in different directions, leading to applicability of three-dimensional stresses including:

- Normal forces for both x and y directions (f_x and f_y)
- In-plane shear forces (f_{xy})
- Transversal force for x and y directions (V_x and V_y)
- Bending moments on both x and y directions (Q_x and Q_y)
- Twisting moment (Q_{xy})

Figure 5-3 have shown abovementioned loads on an element.

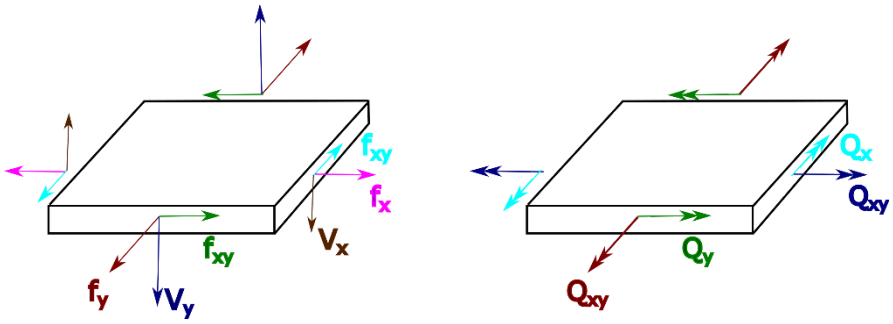

Figure 5-3. Schematic of loads on a single plate element [41].

Each CQUAD4 element is defined by 4 nodes, coordination of the nodes is used in MATLAB to make schematic imported geometry. Element mapping is also needed to show connection of each element to its neighbour elements.

5.3 NASTRAN cards (format) for storing mass and stiffness matrix

Generally NASTRAN consider stiffness matrix to be symmetric, therefore it only store diagonal and lower triangular elements. Array is addressed based on DOFs of each node. Nodes are exist in the Grid which present the geometry can be correlated to DOFs. CQUAD4 element have 4 nodes and each node have 6 DOFs, in total 24 DOFs is counted for each element [42]. To show how NASTRAN construct the stiffness matrix, following matrix is presented for 1 single element:

$$\begin{bmatrix}
(1,1) & & & & & & & & Sym \\
(1,1) & (1,2) & & & & & & & \\
\vdots & \vdots & \ddots & & & & & & \\
(1,1) & (1,2) & \cdots & (1,6) & & & & & \\
(1,1) & (1,2) & \cdots & (1,6) & (2,1) & & & & \\
(1,1) & (1,2) & \cdots & (1,6) & (2,1) & (2,2) & & & \\
\vdots & \vdots & \cdots & \vdots & \vdots & \vdots & \ddots & & \\
(1,1) & (1,2) & \cdots & (1,6) & (2,1) & (2,2) & \cdots & (4,5) & \\
(1,1) & (1,2) & \cdots & (1,6) & (2,1) & (2,2) & \cdots & (4,5) & (4,6)
\end{bmatrix} \equiv \begin{Bmatrix}
Node = 1, DOF = 1 \\
Node = 1, DOF = 2 \\
\vdots \\
Node = 1, DOF = 6 \\
Node = 2, DOF = 1 \\
Node = 2, DOF = 2 \\
\vdots \\
Node = 4, DOF = 5 \\
Node = 4, DOF = 6
\end{Bmatrix} \tag{5.3-1}$$

As presented above, stiffness for each element is compound of 24 by 24 square matrix, also obviously due to three-dimensional properties of element for two axis bending and twisting, stiffness is a full rank matrix.

The geometry of the blade is exported as initial graphics exchange specification (IGES) format from CATIA, then imported as a solid object in Patran and then meshed to make a model of CQUAD4 elements, as it is shown in

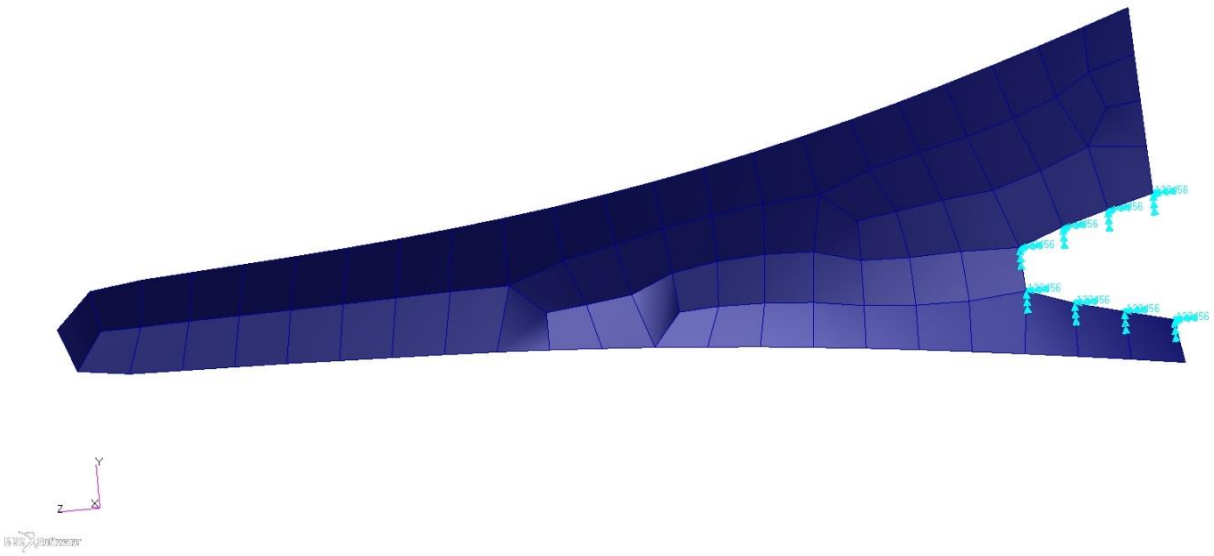

Figure **5-4**.

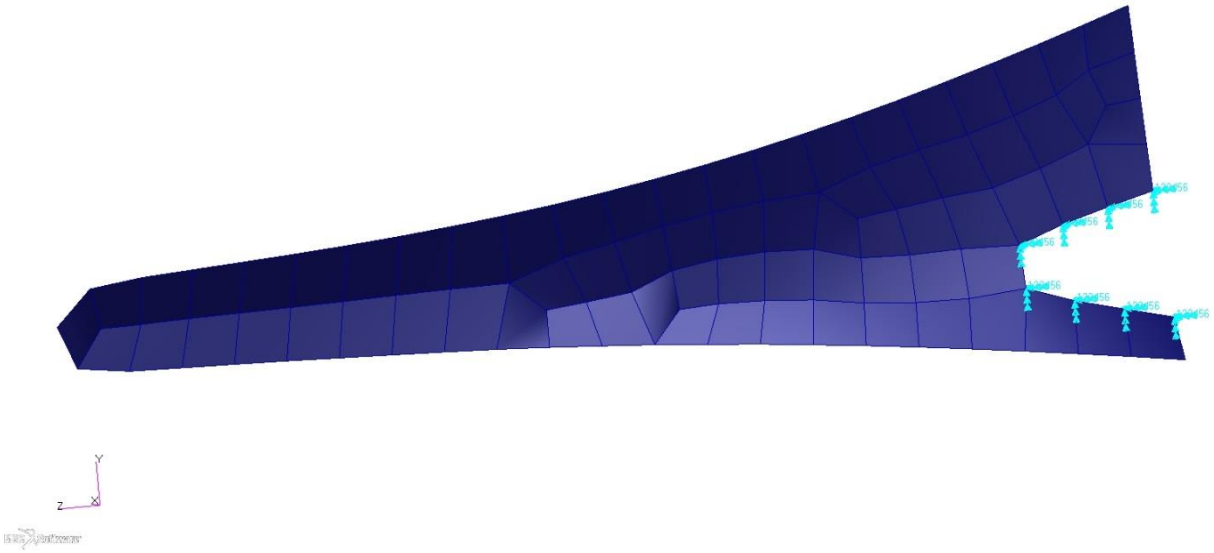

Figure 5-4. Arrangement of the elements for the blade in NASTRAN.

Although some accuracy in geometry of the blade is lost during this conversion, it need to be mentioned that the selection of element type is based on consideration of possible location sensor installation. Obviously, such sensors may not be placed under the surface in laboratory experiments.

5.4 Extraction of the model for MATLAB

To apply Kalman estimator to wind turbine blade, the model need to be presented in mathematical model in MATLAB. Stiffness and mass matrix of the model then will be used in the simulation and obtaining required observations.

The nodes are presented by node numbers and three-dimensional Cartesian coordination. Figure 5-5 is illustrated shape of the blade. Red nodes in the figure are free nodes, cyan nodes are taken interface of the blade with rotor. Model in total contains 101 nodes and subsequently 606 DOFs.

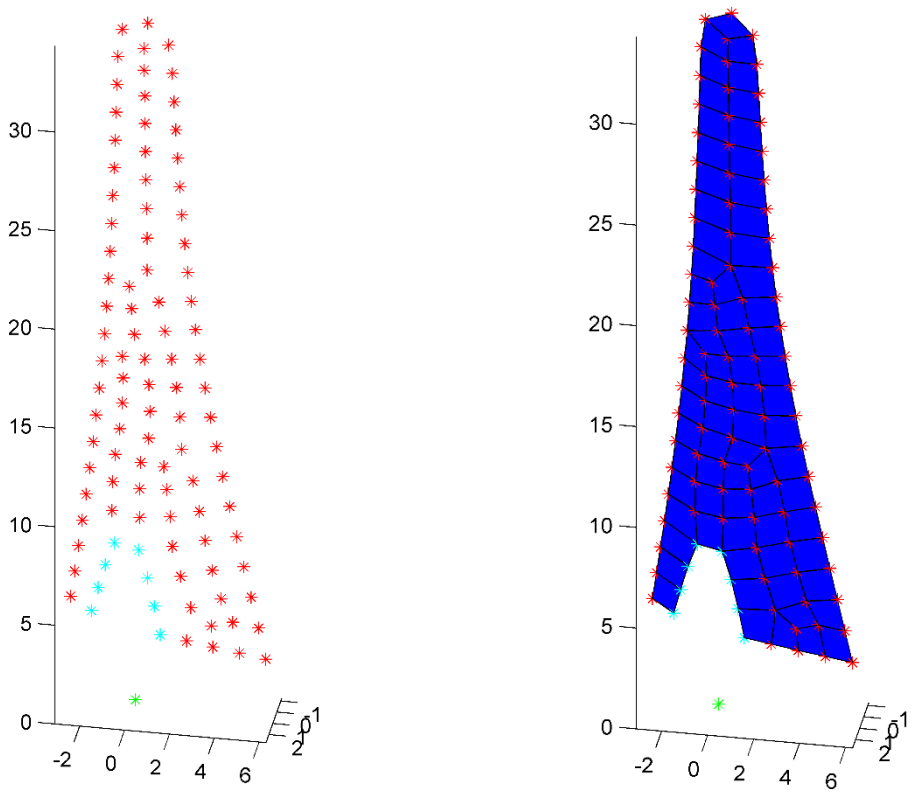

(a) (b)

Figure 5-5. a: Coordination of the nodes for the model mesh in MATLAB b: Schematic of elements in MATLAB.

5.5 Substructuring for tip of the blade

Complete model of the blade consist of 606 DOF which is challenging to handle, also such number of sensors is not feasible to be installed. The tip of the blade is prone to be damaged

during the transportation, therefore here it is assumed area of concern are first five elements of the blade tip. These elements are used in the identification process, in Figure 5-6 these elements are coloured to be distinguishable by blue colour.

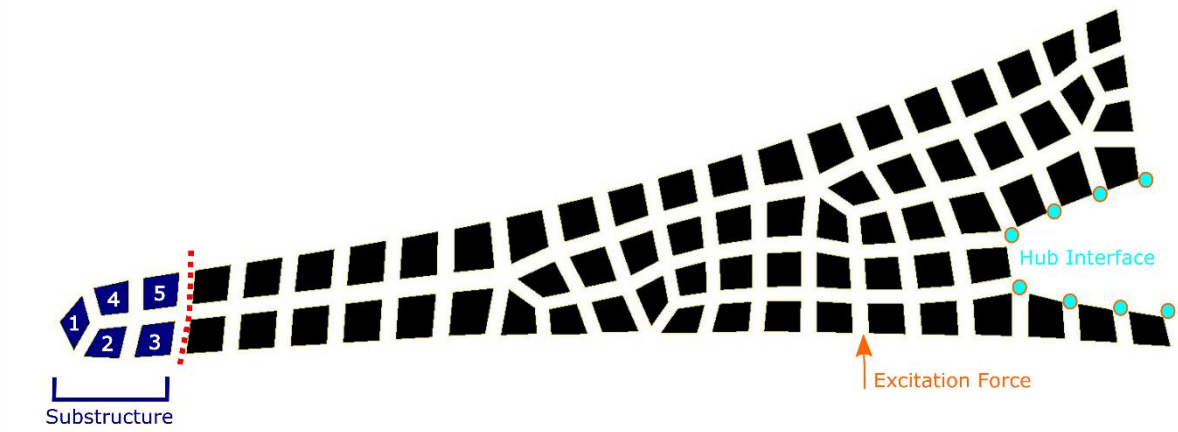

Figure 5-6. Schematic definition the substructure, excitation force and element numbering.

Also they are numbered from 1 to 5, so the result can be addressed to exact location. Meanwhile, node numbering can be founded in Figure 5-7. Excitation force is chosen without any special assumption. Force amplitude is changing arbitrary and is not generated by a mathematical function. There is no restriction for location and number of excitation forces. In laboratory experiments this force can be generated by moving the rotor blade. All free DOFs are excited by the force, except 8 nodes in hub interface which are considered as fixed in this experiment.

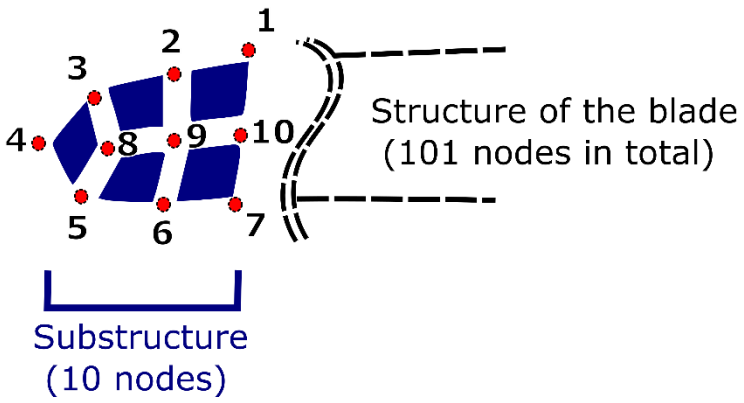

Figure 5-7. Node numbering for the substructure.

Departed part of the blades have 60 DOFs in total which is considerably smaller than the system total DOFs. As result, by few number of DOFs - as much as one tenth of the real model – damage detection process is possible to apply.

Initial guess of the stiffness matrix do not play a role in the estimation, therefore iteration can start with any value as far as it is reasonable numerically. These values as an example can be 20 times more than real simulation.

5.6 Convergence of the system dynamics

Estimation of system dynamics including accelerations, velocities and displacement for substructured part are compared to real simulation in following graphs and result are illustrated in Figure 5-8 to Figure 5-16. It shall be noted that not all the DOFs are converged, in several of them, the amount of error is rather high in comparison with previous chapter, such as seen in Figure 5-12 and Figure 5-16. Measurements which are used for estimation are polluted with 5 percent noise, initial guess covariance matrix is diagonal, although it will not remain diagonal through simulation steps.

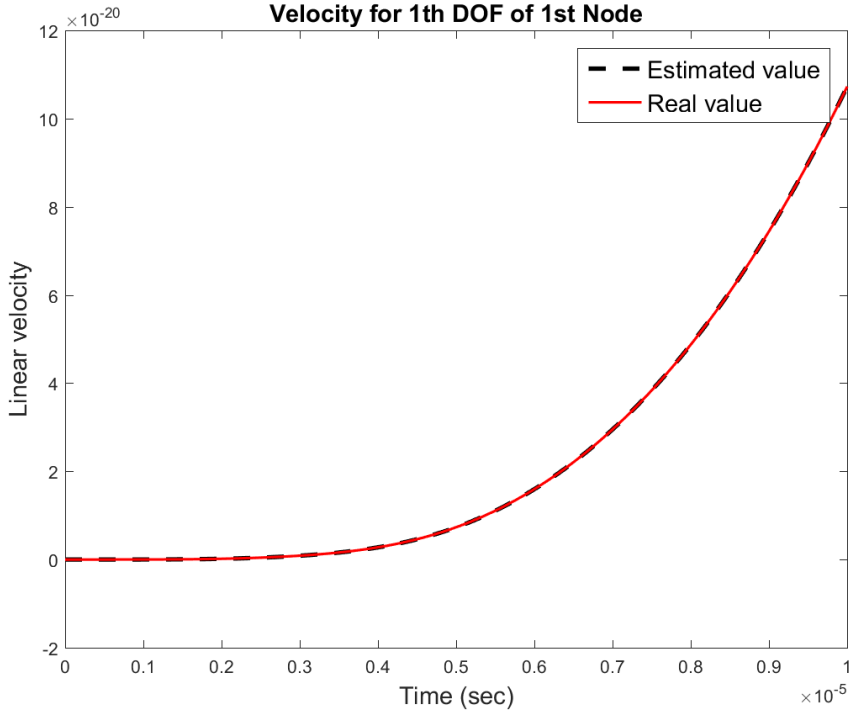

Figure 5-8 Estimation of 1th DOF velocity in 1st node of the substructure in last global loop of iteration in comparison to real value.

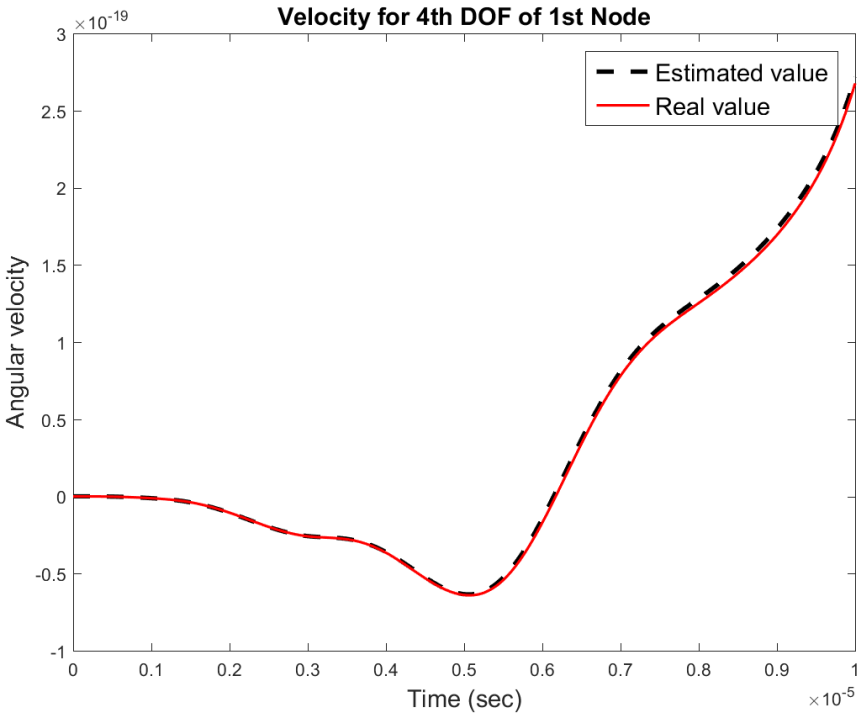

Figure 5-9 Estimation of 4th DOF acceleration in 1st node of the substructure in last global loop of iteration in comparison to real value.

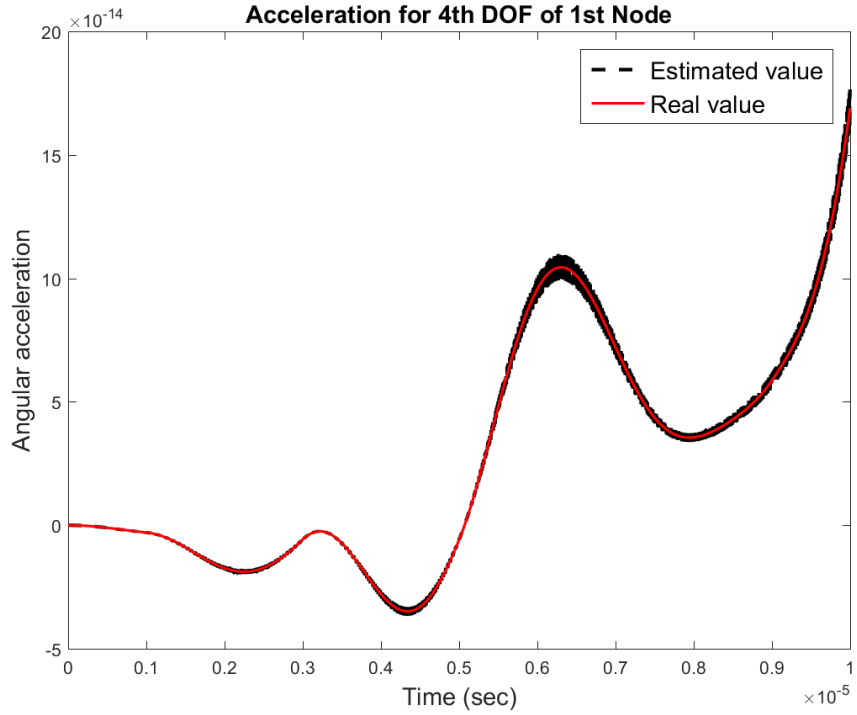

Figure 5-10. Estimation of 4th DOF acceleration in 1st node of the substructure in last global loop of iteration in comparison to real value.

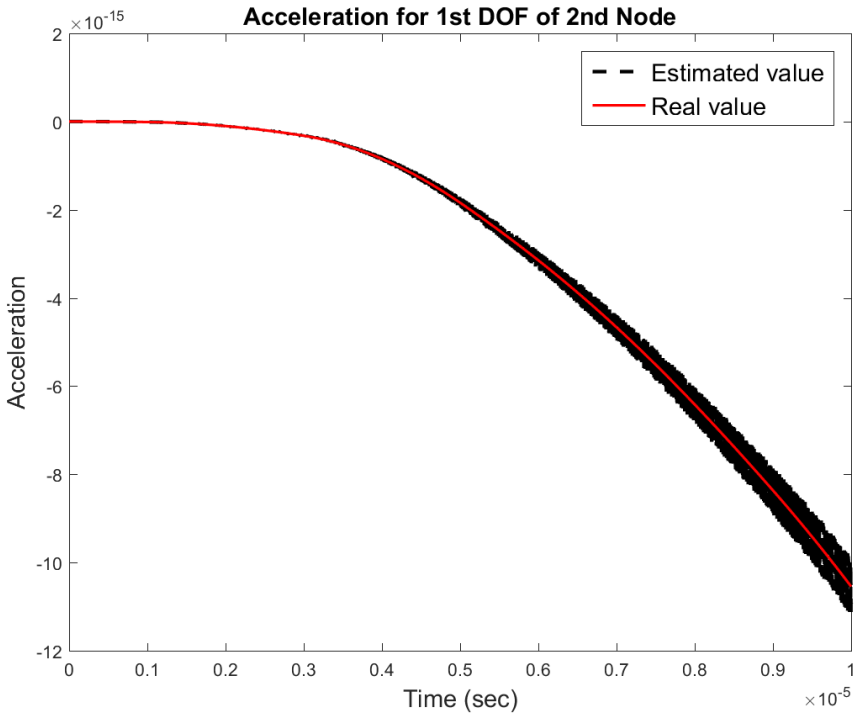

Figure 5-11. Estimation of 1st DOF acceleration in 2nd node of the substructure in last global loop of iteration in comparison to real value.

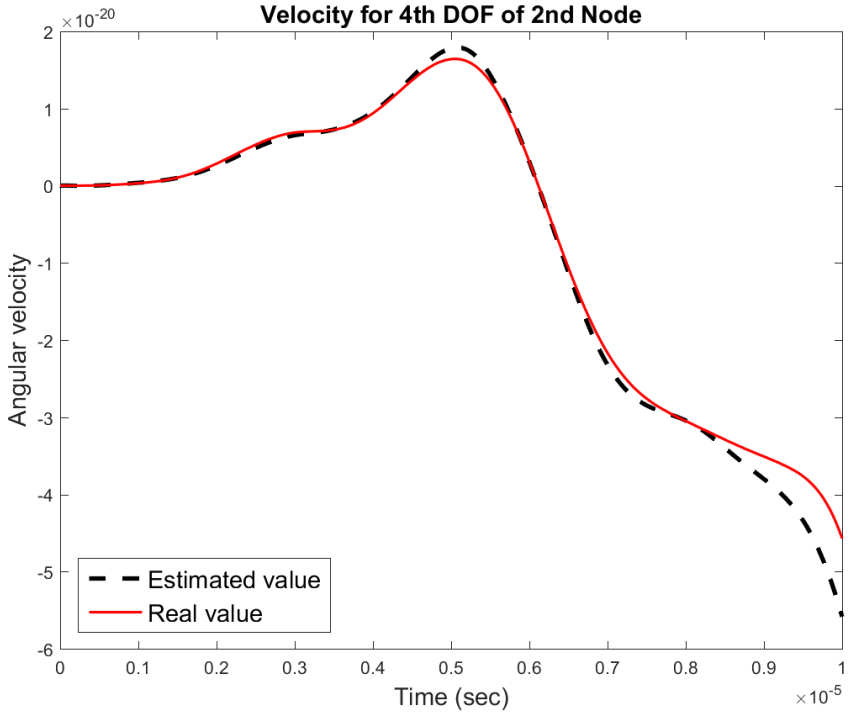

Figure 5-12. Estimation of 4th DOF velocity in 2nd node of the substructure in last global loop of iteration in comparison to real value.

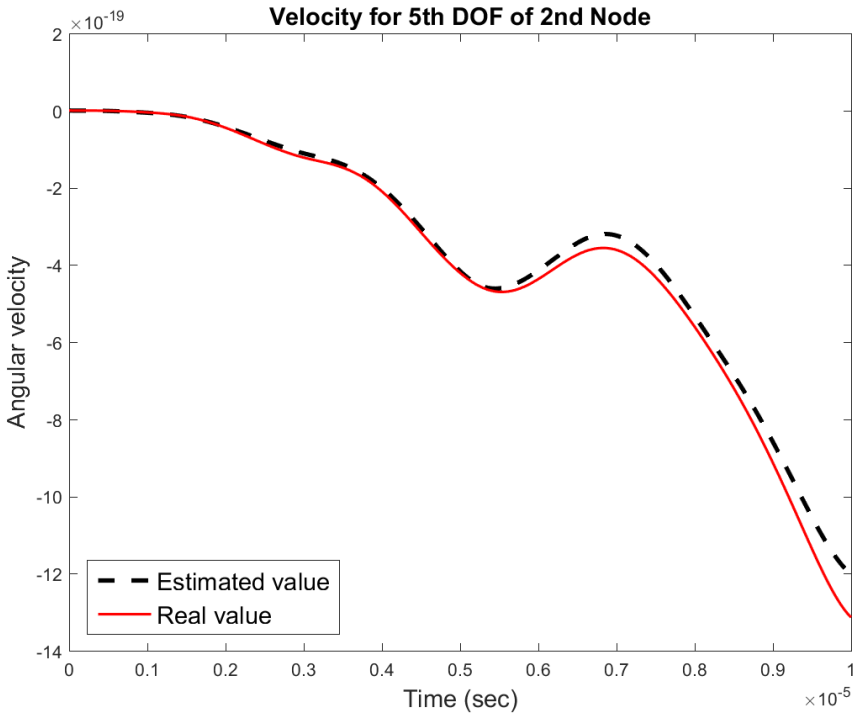

Figure 5-13. Estimation of 5th DOF velocity in 2nd node of the substructure in last global loop of iteration in comparison to real value.

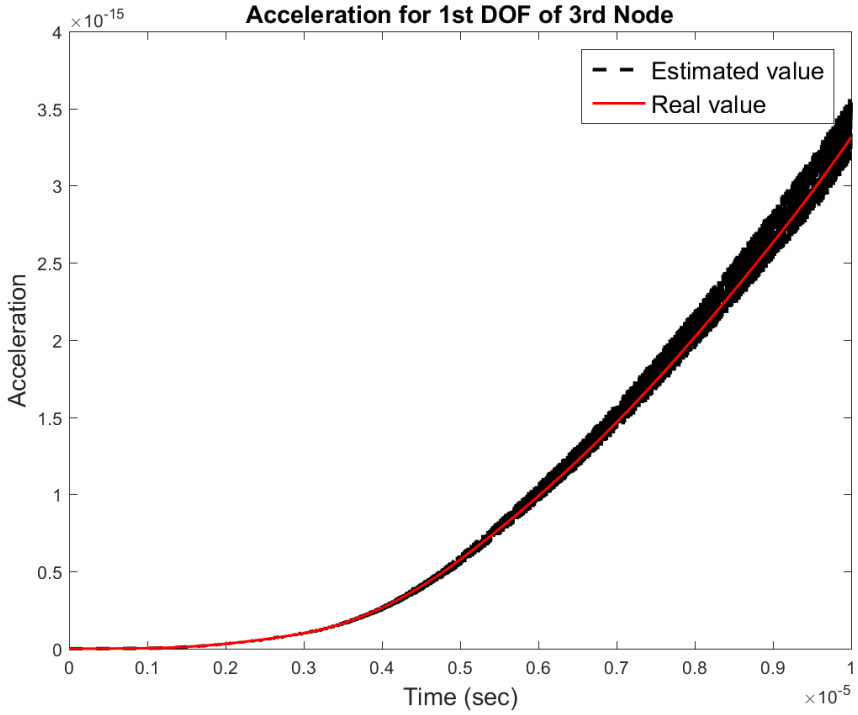

Figure 5-14. Estimation of 1st DOF acceleration in 3rd node of the substructure in last global loop of iteration in comparison to real value.

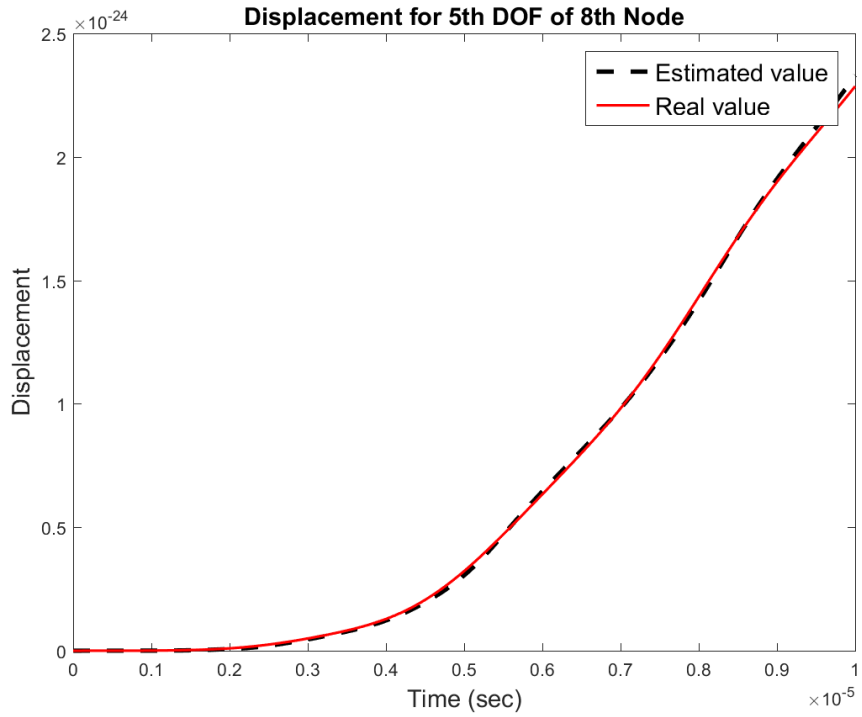

Figure 5-15. Estimation of 5th DOF displacement in 8th node of the substructure in last global loop of iteration in comparison to real value.

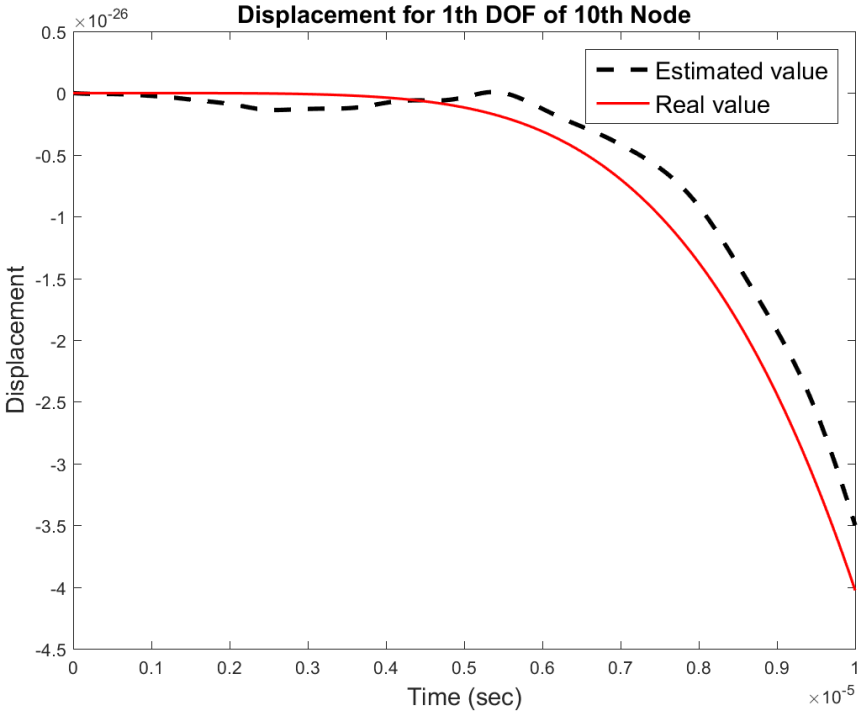

Figure 5-16. Estimation of 1th DOF displacement in 10th node of the substructure in last global loop of iteration in comparison to real value.

Number of global iterations is 100 and each local iteration is consist of 60000 steps, the numerical integration is calculated by finer time steps to assure highest accuracy. Also due to hardware restriction, MATLAB default accuracy was reduced to 16 digits during the iteration. The results are presented in Table 5-1.

Table 5-1. Convergence of the stiffness correlated values for the blade.

Parameter	Real value	Initial guess	Value (120^{th} iteration)
Stiffness correlation factor of k_1	1	15	0.8883
Stiffness correlation factor of k_2	1	20	1.088
Stiffness correlation factor of k_3	1	0.5	0.7829
Stiffness correlation factor of k_4	1	5	1.033
Stiffness correlation factor of k_5	1	10	0.9519

Not all of the results are fully converged to real values, but the final estimated parameter is quite close to the reference value compare to initial guess. Non-optimized weighting or insufficient number of iteration are the probable source of error according to best knowledge of the author. Moreover most of the substructure dynamics, including accelerations, velocities and displacements are good estimation of real values at the last step of global iteration.

6 CONCLUSION AND FUTURE WORK

This study has presented the potential of Kalman estimator for system identification of large mechanical structures. Such process is possible to apply for linear and non-linear mechanical systems, with Rayleigh or viscous damping models. Using substructuring approach, one can model only one part of a complete system, and leave parts which are difficult to model or have complicated boundary conditions. Efficiency of the presented method for damage detection and model updating based on substructuring is outstanding comparing to other previous methods as this method will not take any consideration for whole mechanical system. In this way, damage detection is possible to perform locally and in area of concern, so without losing accuracy, required modelling time is shortened.

The faster and more accurate convergence of the results which presented by accelerating modified Kalman estimator through variable weighting factor is helpful for complicated systems with large number of DOFs. It is noteworthy to mention that the accuracy of the method is not limited in numerical experiments and can be improved through smaller time steps. Naturally this will lead to higher CPU time for iteration loops.

Procedure of estimation can be applied for different Finite Element models, different element types without restrictions. Although amount of required computation cost in this method is still relatively high, the observations data needed to be recorded only once and for very short time. The method remained robust in presence high noise as far as the noise is not biased. The initial guess in this process do not require any presumption, there is not any necessity to obtain a guess within expected range for parameters in start of simulation. As it have shown in through result chapters, first guess can be higher, lower or almost equal to real values, results are reliable when they stay stable through next steps of iteration and making system dynamics fits to measurement at the same time.

Meanwhile for laboratory experiments, one need to consider that sample rate of industrial accelerometer is limited and might make accuracy limit for the method. There are already innovative technologies in current laser vibrometers from companies such as Polytech for high sampling rates. But advances in scanner vibrometers, piezoelectric materials and signal

processing will make better future path for SI methods based on Kalman estimator. So higher mesh which represent the geometry more accurately can be modelled and measured for very fine time steps such as 10^{-9} sec (1000 MHz).

In this study, more realistic model of the system is presented, results have potential to be closer to laboratory test since unlike previous studies, mass matrix is not assumed essentially lumped or diagonal. Subsequently, this method bring more possibility model updating purposes with consistent mass matrix, which clearly lead to better presentation of the structure based on a FEM.

Further development of this technic can be studied through experimental arrangement of the simulations. There were quite many literature which have done the real measurements on shear buildings and 1-DOF coupling structures for civil application, but according to best knowledge of the author, there was not real estimation with complete mass matrix for more complicated mechanical structures like Wind Turbine blades.

In this study, model of wind turbine is only made of one element type blade is made of one material with a solid aerofoil structure. Although for larger turbines, blades are made of different materials, and many internal components such as spar caps, shear webs, leading edge panel, external surface. So core and surface parts need to be modelled by different element types and according to their rule in blade structure. A compound model of blade can be taken into account for further investigation about application of this damage detection method.

As another prospect for extension of this study, it would be possible to optimize number of sensors on a structure. Collecting data from accelerometers and installation of them needs long preparation. Also these sensors are expensive, therefore the mesh size need to be optimized for model estimation.

REFERENCES

1. Ling, X. Linear and nonlinear time domain system identification at element level for structural systems with unknown excitation. Dissertation. USA: Department of Civil Engineering and Engineering Mechanics, 2000. 182 p.

2. Schallhorn, C. & Rahmatalla, S. Crack detection and health monitoring of highway steel-girder bridges. Structural Health Monitoring, 2015. Vol. 14: 3. Pp. 281–99.

3. Haghani, R., Al-Emrani, M. & Heshmati, M. Fatigue-Prone Details in Steel Bridges. Buildings, 2012. Vol. 2: 4. Pp. 456–76.

4. Cruz, P. J. S. & Salgado, R. Performance of Vibration-Based Damage Detection Methods in Bridges. Computer-Aided Civil and Infrastructure Engineering, 2009. Vol. 24: 1. Pp. 62–79.

5. Sakaris, C. S., Sakellariou, J. S. & Fassois, S. D. Vibration-based damage precise localization in three-dimensional structures: Single versus multiple response measurements. Structural Health Monitoring, 2015. Vol. 14: 3. Pp. 300–14.

6. Koh, C. G., Qiao, G. Q. & Quek, S. T. Damage identification of structural members: Numerical and experimental studies. Structural Health Monitoring, 2003. Vol. 2: 1. Pp. 41–55.

7. Quaranta, G., Carboni, B. & Lacarbonara, W. Damage detection by modal curvatures: Numerical issues. Journal of Vibration and Control, 2016. Vol. 22: 7. Pp. 1913–27.

8. Sandia National Laboratories [web document]. Enormous blades could lead to more offshore energy in U.S., 2016. Updated 28.1.2016. [Referred 03.5.2016]. Available: https://share.sandia.gov/news/resources/news_releases/big_blades/#.VyijVnqNbm4

9. Shreiber, J. 2015. University lecturer and researcher, chair of Wind Energy in Technical University Munich. Held on summer semester 2015. Presentation slides: Wind Energy Research in TUM. Technical University Munich, Germany. Presentation for recent wind energy developments.

10. D7 Platform brochure. 2015. [Siemens webpage]. Published 2015. [Reffered 5.5.2016]. Available: http://www.energy.siemens.com/hq/pool/hq/power-generation/renewables/wind-power/platform%20brochures/D7-Platform-brochure_en.pdf

11. Bottasso, C. L. & Bortolotti, P. 2015 Praktikum Design of Wind Turbine Rotors, Technical University of Munich, Germany. Course lecture slides for summer semester 2015.

12. Yan, Y. J., Cheng, L., Wu, Z. Y. & Yam, L. H. Development in vibration-based structural damage detection technique. Mechanical Systems and Signal Processing, 2007. Vol. 21: 5. Pp. 2198–211.

13. Pizzinga A. Restricted Kalman filtering: Theory, methods, and application. New York: Springer, 2012. 62 p.

14. Oller, S. [Chapter 3:] Solution of Equation of Motion In: Oller, S. Nonlinear dynamics of structures: Springer, 2014. Pp. 29-51.

15. Géradin, M. & Rixen, D. [Chapter 7:] Direct Time-Integration methods In: Geradin, M. & Rixen, D. J. Mechanical vibrations: theory and application to structural dynamics. Third Edition. John Wiley & Sons, 2014. Pp. 518-24.

16. Rixen D. 2015 Structural Dynamics course. University lecturer and researcher, chair of Applied Mechanics in Technical University Munich, Germany. Lecture notes for Structural Dynamics course in summer semester 2015.

17. Lefebvre, T., Bruyninckx, H. & Schutter, J. [Chapter 4:] Kalman Filter for Nonlinear Systems In: Lefebvre, T., Bruyninckx, H. & de Schutter, J. Nonlinear Kalman filtering for force-controlled robot tasks. Springer-Verlag Berlin, 2004. Pp. 51-53.

18. Crassidis, J. L. & Junkins, J. L. Optimal estimation of dynamic systems. 2nd Edition Boca Raton, Fla. London: Chapman & Hall/CRC, 2012. 749 p.

19. Hartikainen, J., Solin, A. & Särkkä, S. Optimal filtering with Kalman filters and smoothers [web document]. Aalto University School of Science 2011, [Referred 05.03.2016] Available: http://becs.aalto.fi/en/research/bayes/ekfukf/documentation.pdf

20. Quek, S. T., Wang, W. & Koh, C. G. System identification of linear MDOF structures under ambient excitation. Earthquake engineering & structural dynamics, 1999. Vol. 28: 1. Pp. 61–77.

21. Hsieh, C. S. & Chen, F. C. Optimal solution of the two-stage Kalman estimator. Automatic Control, IEEE Transactions on 1999. Vol. 44: 1. Pp. 194–9.

22. Alouani, A. T., Xia, P., Rice, T. R. & Blair, W. D. On the optimality of two-stage state estimation in the presence of random bias. IEEE Trans. Automat. Contr., 1993. Vol. 38: 8. Pp. 1279–83.

23. Friedland B. Treatment of bias in recursive filtering. IEEE Trans. Automat. Contr., 1969. Vol. 14: 4. Pp. 359–67.

24. Hoshiya, M. & Sutoh, A. Extended Kalman filter-weighted local iteration method for dynamic structural identification. In: Proceedings of the tenth world conference on Earthquake Engineering, 1992. Pp. 3715–20.

25. Oreta, Andres W. C., Tanabe & T. A. Localized identification of structures by Kalman filter. In: PROCEEDINGS-JAPAN SOCIETY OF CIVIL ENGINEERS, 1993. Vol. 9: 4. Pp. 217-25.

26. Al-Hussein, A. & Haldar, A. A comparison of unscented and extended Kalman filtering for nonlinear system identification, 2015. [12th International Conference on Applications of Statistics and Probability in Civil Engineering, ICASP12].

27. Lei, Y., Liu, C., Jiang, Y. Q., Mao & Y. K. Substructure based structural damage detection with limited input and output measurements. Smart Structures and Systems, 2013. Vol. 12: 6. Pp. 619–40.

28. Lei, Y., Jiang, Y. & Xu, Zh. Structural damage detection with limited input and output measurement signals. Mechanical Systems and Signal Processing, 2012. Vol. 28. Pp. 229–43.

29. Feng, J., Fan, H. & Tse, C. K. Convergence Analysis of the Unscented Kalman Filter for Filtering Noisy Chaotic Signals. In: 2007 IEEE International Symposium on Circuits and Systems. Pp. 1681–4.

30. F. Haugen, Lecture notes in models, estimation and control [web document] Published 2009. [Referred 9.5.2016]. Available: http://www.nb.no/nbsok/nb/65e7359e089657f08c5c960c340638a3?lang=no

31. Wang, D. & Haldar, A. Element-level system identification with unknown input. Journal of Engineering Mechanics, 1994. Vol. 120: 1. Pp. 159–76.

32. Gander W. [Chapter 9:] Simulation In: Gander, W. Learning MATLAB: A Problem Solving Approach. Springer, 2015. Volume 95 of the series UNITEXT. Pp. 79-97.

33. Mikkola A. University lecturer and researcher. Lecture notes for Machine Simulation Laboratory course. Lappeenranta University of Technology, Finland, 2015. Machine Simulation Laboratory course.

34. Cook, R. D. [Chapter 2:] One-dimensional elements and computational procedures. In: Cook, R. D., Malkus, D. S., Plesha, M. E. & Witt, R. J. Concepts and applications of finite element analysis. 4th Edition. John Wiley & Sons, 2007. Pp. 19-77.

35. Dumont, M. & Kinsley, N. Rotational Accelerometers and Their Usage in Investigating Shaker Head Rotations. In: Dumont, M. & Kinsley, N. (editors). Sensors and Instrumentation. Volume 5. Springer, 2015. Pp. 85–92.

36. Roettgen, D. R. & Mayes, R. L. Ampair 600 Wind Turbine Three-Bladed Assembly Substructuring Using the Transmission Simulator Method. In: Allen, M., Mayes, R. L., Rixen, D. J., editor. Dynamics of Coupled Structures, Volume 4. Cham: Springer International Publishing, 2015. Pp. 111–23 [Conference Proceedings of the Society for Experimental Mechanics Series].

37. Mayes R., Rixen D., Griffith D. T., Klerk, D. de, Chauhan, S., Voormeeren, S. N. & Allen, M. S. Topics in Experimental Dynamics Substructuring and Wind Turbine Dynamics, Volume 2: Proceedings of the 30th IMAC, A Conference on Structural Dynamics, Springer Science & Business Media, 2012.

38. Gross, J., Oberhardt, T., Reuss, P. & Gaul, L. Model updating of the Ampair wind turbine substructures. In: Proceedings of the 32th international modal analysis conference, 2014.

39. Mayes, R. L. An Introduction to the SEM Substructures Focus Group Test Bed – The Ampair 600 Wind Turbine. Topics in Experimental Dynamics Substructuring and Wind Turbine Dynamics, Volume 2. New York, Springer, 2012. Pp. 61–70 [Conference Proceedings of the Society for Experimental Mechanics Series].

40. Ampair 600 Wind Turbine: Operation, Installation and Maintenance Manual, 2007. [Ampair and Boost Energy Systems Ltd. webpage], Published July 2007. [Referred 19.5.2016]. Available: http://www.hispaniasolar.es/pdf/Ealternativas/Ampair600.pdf.

41. MSC Nastran 2012 Linear Static Analysis User's Guide, 2012. [MSC Nastran webpage]. Updated 23.11.2011 [Referred 20.5.2016]. Available from: https://simcompanion.mscsoftware.com/infocenter/index?page=content&cat=MSC_NASTRAN_DOCUMENTATION_2012&channel=DOCUMENTATION.

42. MSC Nastran 2016 Reference Manual, 2016. [MSC Nastran webpage]. P June 2016. [Referred 24.5.2016]. Available: https://simcompanion.mscsoftware.com/resources/sites/MSC/content/meta/DOCUMENTATION/10000/DOC10967/~secure/msc_nastran_2016_reference_manual.pdf?token=tfGw2LhT2aZZ4MlBNYFFyxnQDRHqHQVvuYYpKkOevhlX!P8vi-A!bBZ6Ho3ekxYY-wlkmk16GCYxW8lA9l7HXQp804PGG6xF5T5bllH4jT!pYBdmYGSsOFB2RocNWW8Gjolt1cIgDP23jd!DWSh4zTlVHpK!sS496EcakudxCCTDPGpzRO0YQ2rDRv3B1reXxU7kPUFayl4PpD4Dc-8mxwygGxWcu22C5A9Hmip1!DHiKhhGoLGigkHYRWuRcBw!.

Convergence of Kalman global iteration for all time steps in 10 stages.

Following graphs illustrate how Kalman estimator converge to exact estimation for one sample chosen acceleration, while each figure is made of 20000 time steps.

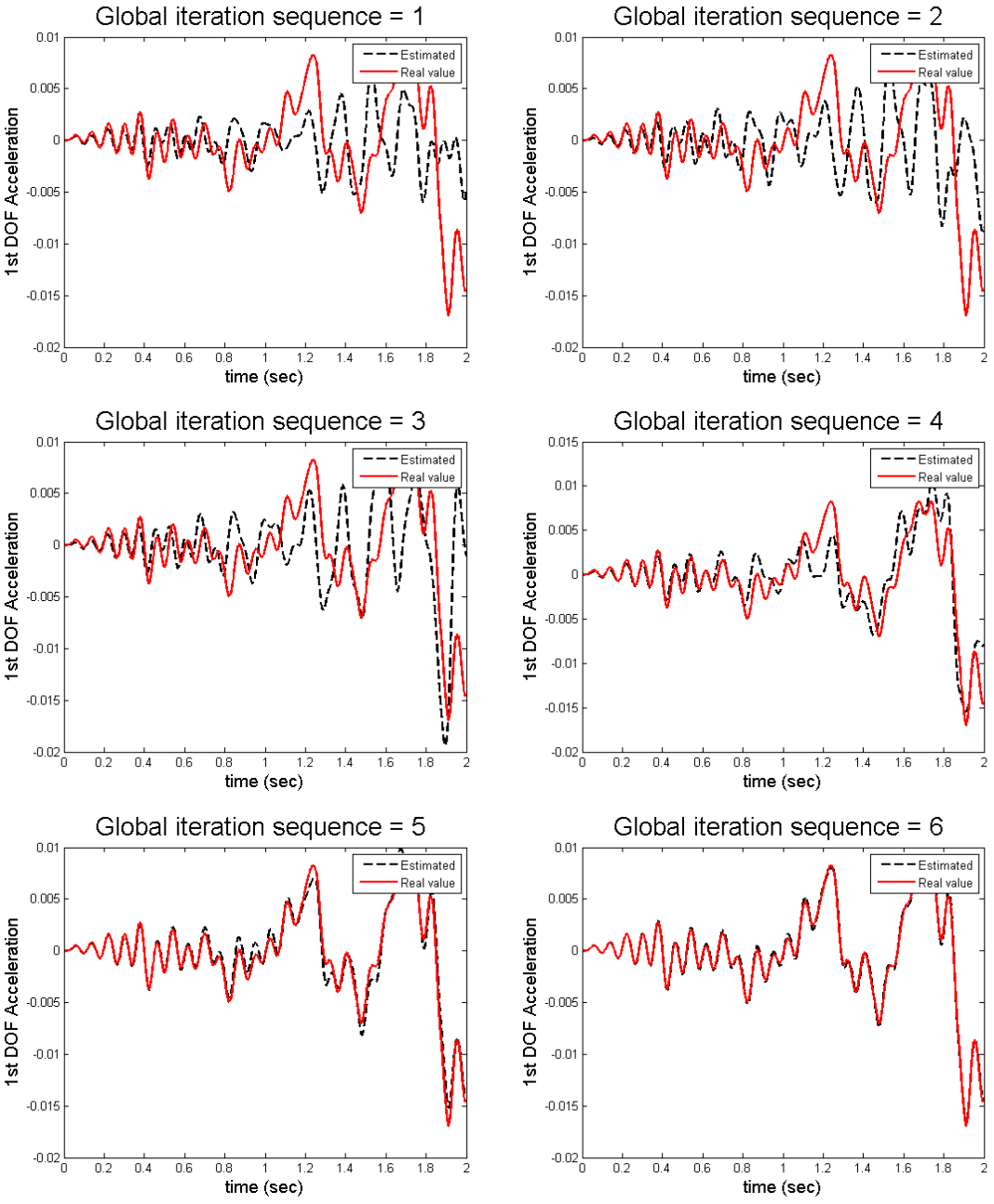

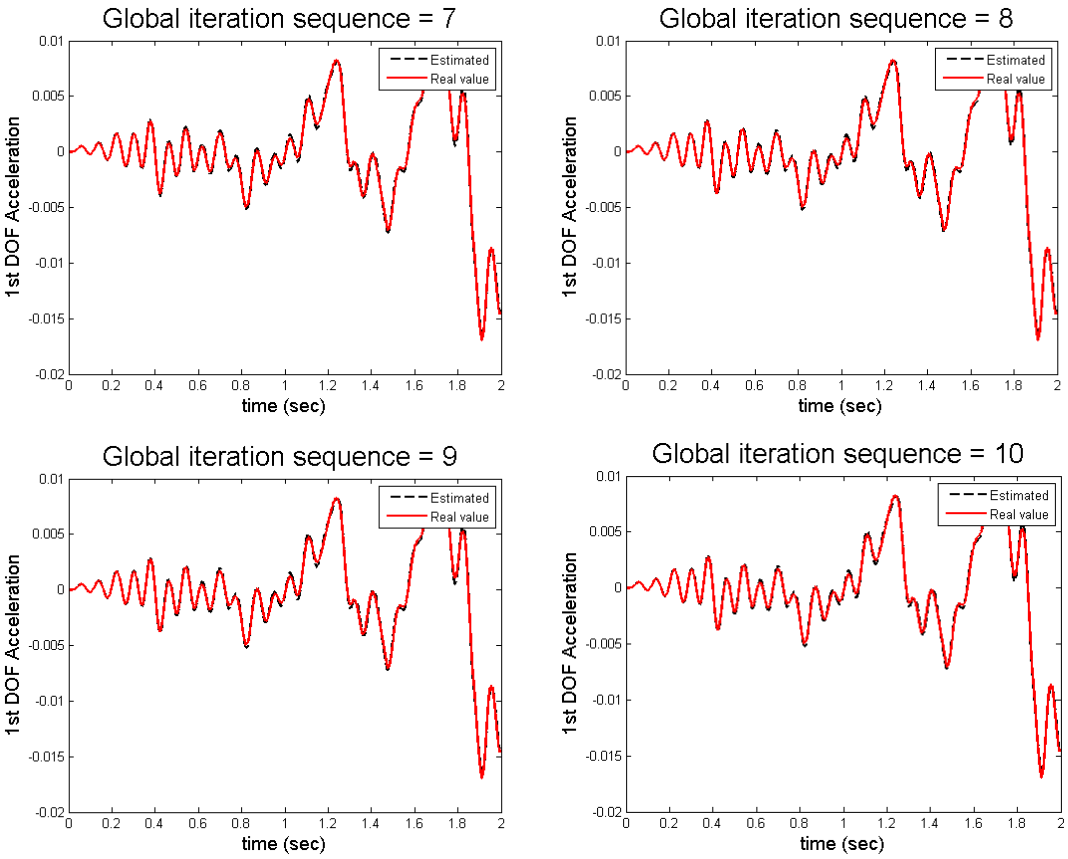
Global iteration sequence = 7
Global iteration sequence = 8
Global iteration sequence = 9
Global iteration sequence = 10
Estimated
Real value
1st DOF Acceleration
time (sec)
0.01
0.005
0
-0.005
-0.01
-0.015
-0.02
0
0.2
0.4
0.6
0.8
1
1.2
1.4
1.6
1.8
2

Convergence of force estimation process for substructured beam with non-diagonal mass matrix.

Force estimation convergence is shown in following steps for a substructured beam consist of 3 elements and considering non-diagonal mass matrix, including global iteration numbers 1 to 8, 10, 20, 30, 40, 100 and 200.

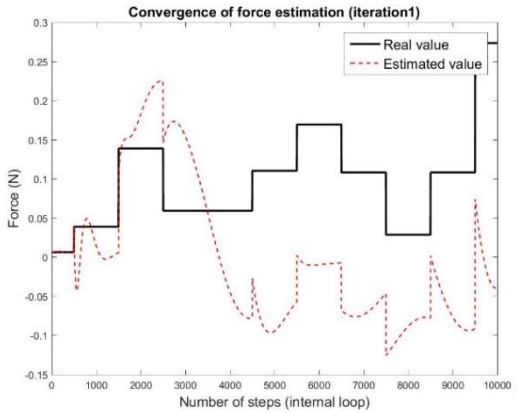

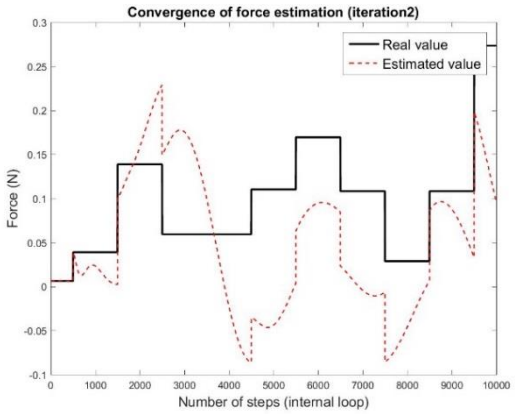

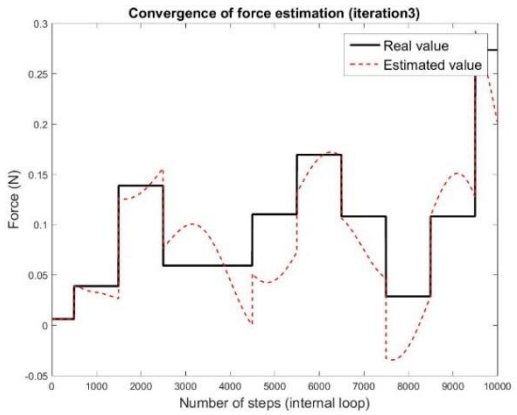

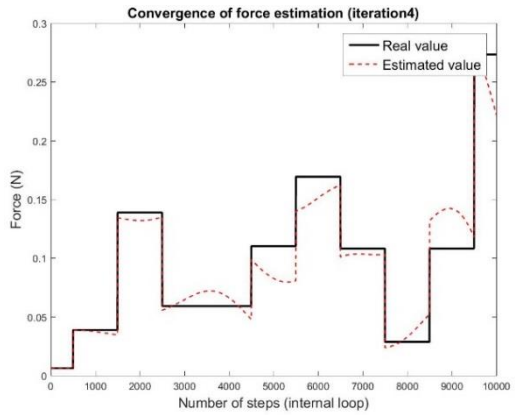

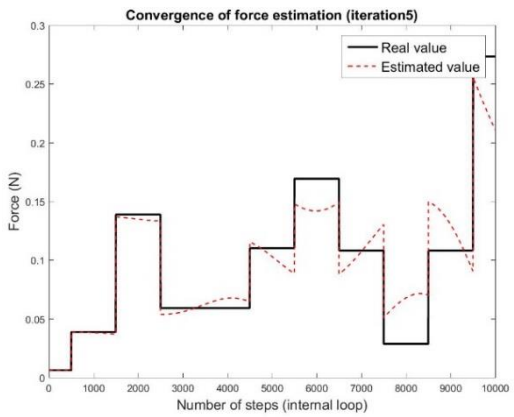

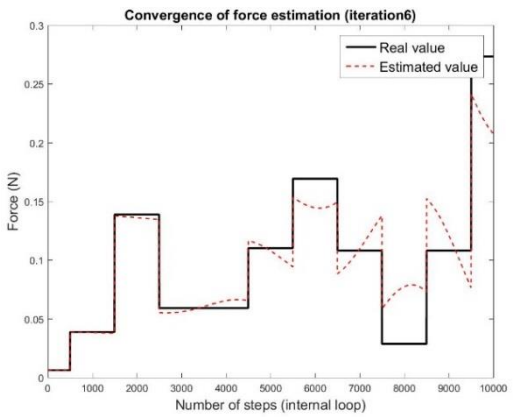

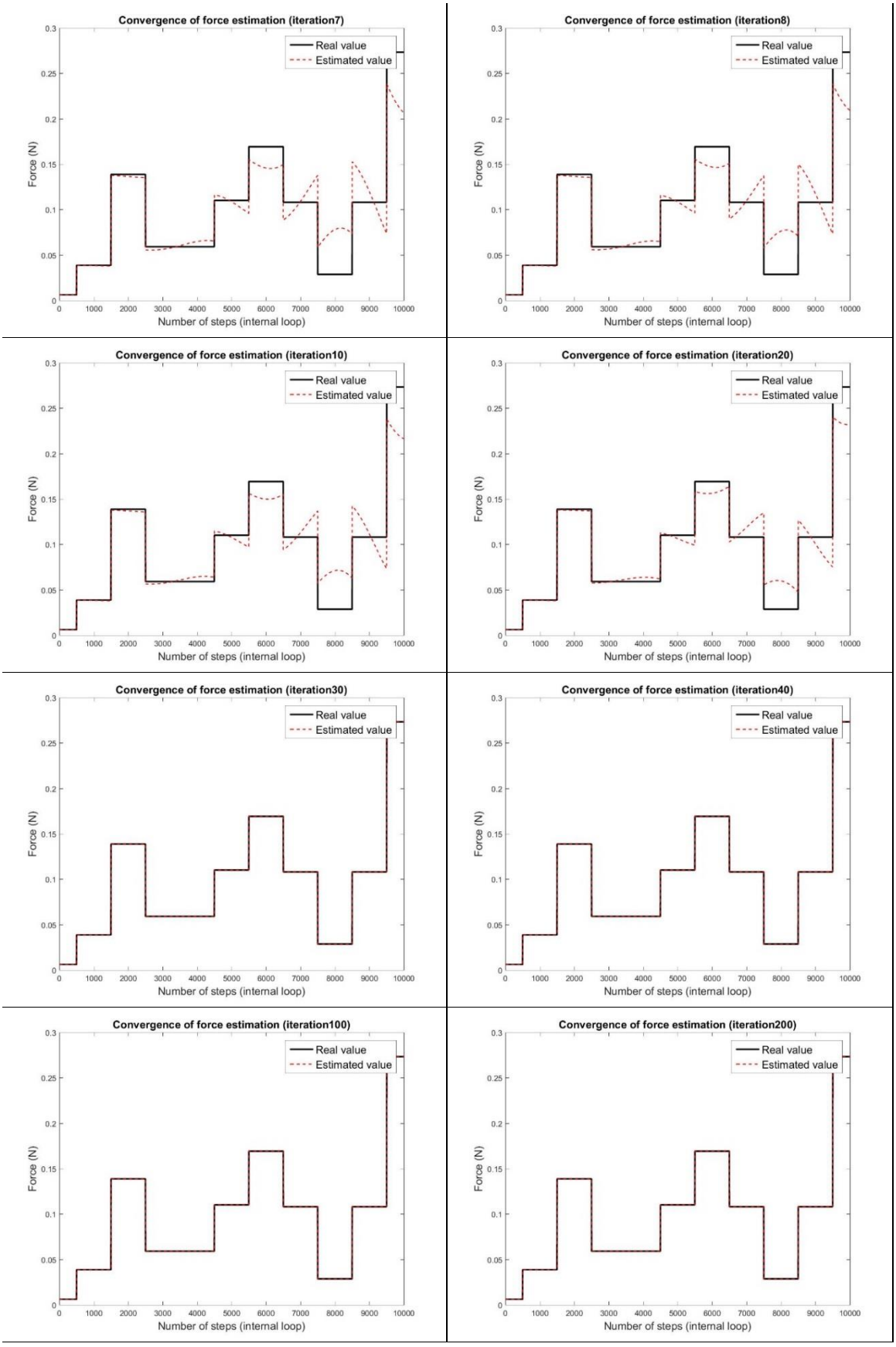
Convergence of force estimation (iteration7)
Convergence of force estimation (iteration8)
Convergence of force estimation (iteration10)
Convergence of force estimation (iteration20)
Convergence of force estimation (iteration30)
Convergence of force estimation (iteration40)
Convergence of force estimation (iteration100)
Convergence of force estimation (iteration200)
Real value
Estimated value
Force (N)
Number of steps (internal loop)